Article

A Criterion for Rating the Usability and Accuracy of the One-Diode Models for Photovoltaic Modules

Aldo Orioli * and Alessandra Di Gangi

DEIM Dipartimento di Energia, Ingegneria dell'Informazione e Modelli Matematici,
Università degli Studi di Palermo, Viale delle Scienze Edificio 9, Palermo 90128, Italy;
alessandradigangi@dream.unipa.it

* Correspondence: orioli@dream.unipa.it; Tel.: +39-091-2386-1905; Fax: +39-091-484-425

Abstract: In selecting a mathematical model for simulating physical behaviours, it is important to reach an acceptable compromise between analytical complexity and achievable precision. With the aim of helping researchers and designers working in the area of photovoltaic systems to make a choice among the numerous diode-based models, a criterion for rating both the usability and accuracy of one-diode models is proposed in this paper. A three-level rating scale, which considers the ease of finding the data used by the analytical procedure, the simplicity of the mathematical tools needed to perform calculations and the accuracy achieved in calculating the current and power, is used. The proposed criterion is tested on some one-diode equivalent circuits whose analytical procedures, hypotheses and equations are minutely reviewed along with the operative steps to calculate the model parameters. To assess the achievable accuracy, the current-voltage (*I-V*) curves at constant solar irradiance and/or cell temperature obtained from the analysed models are compared to the characteristics issued by photovoltaic (PV) panel manufacturers and the differences of current and power are calculated. The results of the study highlight that, even if the five parameter equivalent circuits are suitable tools, different usability ratings and accuracies can be observed.

---

1. Introduction

In the field of photovoltaics, the diode-based equivalent circuits of photovoltaic (PV) cells and modules have been widely used because they allow the designer to optimize the system performance and maximize the effectiveness of the economic investment. The use of accurate models of the electrical behaviour of PV modules, which is obviously important to implement simulation tools, is also required to test the dynamic performances of the inverters equipped with the maximum power point tracker (MPPT). In order to get results, which would be confirmed by experimental measurements, the practical effectiveness of MPPT control algorithms was analysed using different diode-based equivalent circuits [1–3]. It was observed that the study of the transient conditions, which are quite common for an MPPT, requires very reliable equations describing the behaviour of the PV array working far from the standard rating conditions [4].

Usability and accuracy, which have been already addressed by other authors [5], are important features that have to be carefully considered before deciding the mathematical model to be adopted to simulate the electrical behaviour of PV devices. The usability is mainly affected by the mathematical difficulties, which may be encountered in performing calculations, and the unavailability of the performance data used to evaluate the model parameters. Before starting working, it would be preferable to have a clear idea about the need of specific performance data, which may be not available

or difficult to extract from the issued datasheets, and the computation difficulties, which may require the use of mathematical tools ranging from simple algorithms to complex methods implemented in dedicated computational software. Also the accuracy is a relevant parameter, even though its achievable level may significantly depend on the physical characteristics of the modelled PV devices.

To better understand the origin of the diode-based equivalent circuits used for modelling PV devices it is useful to remember that, like a semiconductor diode, a PV cell consists of two layers of semiconductor material, usually silicon, differently doped, that are electrically connected to two metallic electrodes deposited on their outer surfaces. To better understand the origin of the diode-based equivalent circuits used for modelling PV devices it is useful to remember that a PV cell is a diode made with two layers of semiconductor material, usually silicon, differently doped, that are electrically connected to two metallic electrodes deposited on their outer surfaces. It is well-known [2,6] that the absorption of light in semiconductors can, under certain conditions, create an electric current due to the capability of the absorbed photons of converting fixed electrons in freely moving conduction electrons.

A silicon PV cell shares with semiconductor electronic devices, such as diodes and transistors, the same processing and manufacturing techniques used to create p-n junctions. An ideal PV cell behaves like an illuminated semiconductor diode whose *I-V* characteristic was described by Shockley [7] with the following equation:

$$I = I_L - I_0 \left(e^{\frac{qV}{\gamma kT}} - 1 \right) \tag{1}$$

where *I* and *V* are the current and voltage, I_L is the photocurrent generated by illumination, I_0 is the reverse saturation current of the diode, *q* is the electron charge (1.602×10^{-19} C), *k* is the Boltzmann constant (1.381×10^{-23} J/K), *T* is the junction temperature and diode ideality factor γ, in compliance with the traditional theory of semiconductors [8], is 1 for germanium and approximately 2 for silicon.

Wolf [9] observed that in a PV cell the photocurrent is not generated by only one diode but it is the global effect of the presence of a multitude of elementary flanked diodes that are uniformly distributed throughout the surface that separates the two semiconductor slabs of the p-n junction. The assertion of Wolf arises from a significant difference between diodes and PV cells: unlike semiconductor diodes, the upper electrode of a PV cell is deposited with a discontinuous structure that embeds several metal elements (fingers), whose shape and size are chosen with the aim of maximizing the absorbing surface and minimizing the contact resistance between fingers and silicon. In a real diode the electrodes face each other and the carriers of electricity flow through the silicon slabs following linear paths, which are perpendicular to the junction. In contrast, into a PV cell, because of the discrete shape of the upper electrode, the carriers of electricity follow curved paths toward the fingers that collect them (Figure 1).
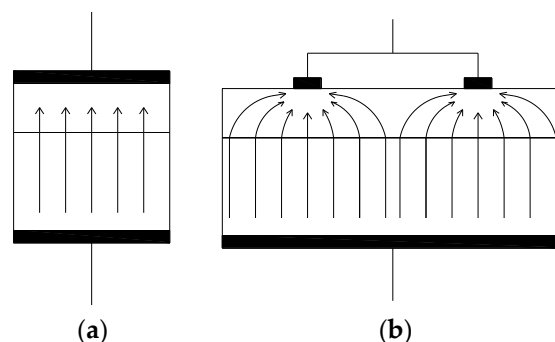

(**a**)   (**b**)

Figure 1. Schematic electrical charges flow paths (**a**) in a diode and (**b**) in a photovoltaic (PV) cell.

As a result of the unequal length of the current paths, the carriers of electricity flow through different thicknesses of semiconductor and different electrical resistances are thus opposed. As consequence, each elementary portion of the p-n junction has a different electrical behaviour and, in turn, a different *I-V* characteristic. In order to get a realistic representation, a PV cell may be

approximated with the distribute constants electric circuit of Figure 2, which contains a multitude of elementary lumped components composed of a current generator and a diode. Numerous electrical resistances take account of various dissipative effects. Major contributions to the internal series resistance come from the sheet resistance of the p-layer, the bulk resistance of the n-layer and the resistance between the semiconductor layers and the metallic contacts.
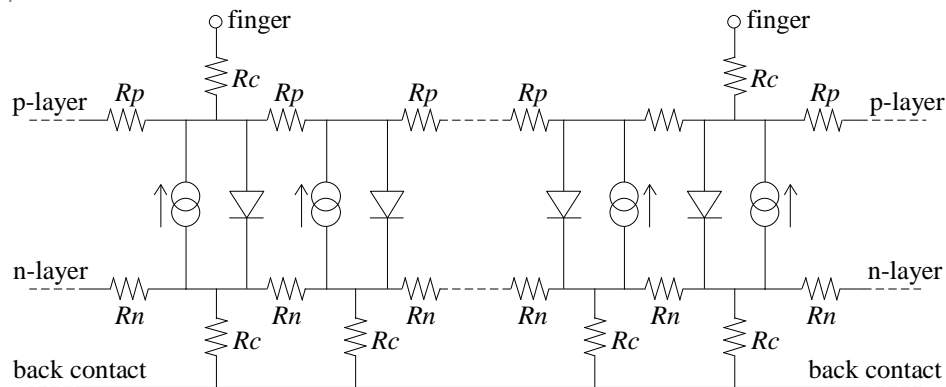

Figure 2. Distributed constant equivalent circuit.

The elementary diodes are inter-connected by resistors R_p and R_n, which represent the transverse distributed resistances of p-layer and n-layer, respectively; resistors R_c are included to consider the contact resistance between the semiconductor and the fingers, or the back contact. Because such equivalent circuit would be too complex to be used, simplified equivalent circuits, which contain one or two diodes, a current generator and two resistors, were considered.

Many authors have proposed analytical procedures for determining the model parameters on the basis of the performance data usually provided by manufactures [10–57]. The identification of the parameters contained in the diode-based equivalent circuits has been also tackled exploring the possibility of using different procedures such as Lambert *W*-function, evolutionary algorithms, Padè approximants, genetic algorithms, cluster analysis, artificial neural networks, harmony search-based algorithms and small perturbations around the operating point [58–69]. One-diode and two-diode models have been also used to describe the electrical behaviour of PV modules built with different technologies, such as thin-film PV cells and panels [17,18,47,49,66,70–82].

Because of the amount of combinations that can be obtained by changing the used set of performance data, the adopted hypotheses and the analytical procedures for evaluating the model parameters, a great number of one-diode models have been reported in the scientific literature. The selection of the model fit for purpose may be a difficult task, which cannot disregard some important aspects, such as:

- the kind and availability of the performance data used by the model;
- the reliability of the hypotheses on which the model is based;
- the procedure followed to obtain the expressions used to calculate the model parameters;
- the mathematical methods, tools and/or computer routines required to solve the equation system;
- the robustness and stability of the mathematical approach;
- the achievable precision of the model.

The features mentioned above affect the model effectiveness and change its usability rating and accuracy level. The usability is a qualitative parameter, whereas the accuracy achievable by a model requires a quantitative assessment. An aware choice of the one-diode model, which should be the best compromise between analytical complexity and expected accuracy, would require the capability of performing the complex synthesis of both qualitative and quantitative features. In order to help

researchers and designers, working in the area of photovoltaic systems, to select the model fit for purpose, the usability and accuracy of some of the most famous one-diode models are overviewed and rated in this study. The paper is organised as follows: Section 2 presents the five-parameter equivalent circuit. To assess the usability rating the analytical procedures of some one-diode models are synthetically reviewed in Section 3 along with the used performance data, the required mathematical tools and the operative steps to obtain the model parameters. In Section 4, the accuracy of the tested one-diode models is evaluated by calculating the *I-V* characteristics of some PV modules and comparing them with the performance curves issued by manufacturers. A criterion for rating the usability and accuracy of the analysed one-diode models is presented in Section 5. Moreover, the model, which represents the ideal compromise between the usability and accuracy is highlighted. The appendix lists the detailed descriptions of the procedures used by the ranked models and the explicit or implicit expressions necessary to evaluate the model parameters; such a review also contains the sequence of operative steps to easily calculate the model parameters.

2. The One-Diode Equivalent Circuit

The one-diode equivalent circuit depicted in Figure 3 is characterized by five parameters, which are photocurrent I_L, diode reverse saturation current I_0, series resistance R_s, shunt resistance R_{sh}, and diode quality factor $n = aN_{cs}k/q$, in which a is the shape factor, N_{cs} is the number of cells of the panel that are connected in series, q is the electron charge (1.602×10^{-19} C) and k is the Boltzmann constant (1.381×10^{-23} J/K).
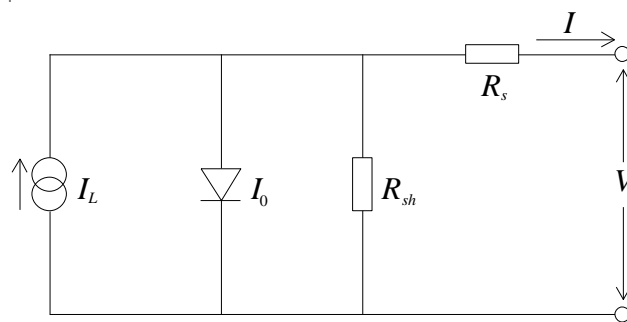

Figure 3. One-diode equivalent circuit for a PV panel.

The one-diode model is described by the well-known equation:

$$I = I_L - I_0 \left(e^{\frac{V + IR_s}{nT}} - 1 \right) - \frac{V + IR_s}{R_{sh}} \tag{2}$$

where T is the cell temperature. Following the traditional theory, the photocurrent depends on the solar irradiance and the diode reverse saturation current is affected by the cell temperature. The values of R_s, R_{sh}, n and I_0 variously affect the *I-V* characteristic of the PV panel [83]. The series and shunt resistances take account of dissipative phenomena and parasitic currents within the PV panel.

At a constant value of the solar irradiance, the internal dissipation of energy is reduced if the series resistance is lowered and/or the shunt resistance is increased. As a consequence, the panel becomes more efficient because the maximum power point (MPP) slides towards right and the *I-V* curve becomes sharper. Thin-film PV cells and modules, which present significant values of R_s and R_{sh} due to the use of materials that are more energy dissipative than the mono or poly crystalline silicon, are usually characterized by smooth *I-V* curves.

The analytical procedures proposed to calculate the five-parameter model generally require the following data, some of them are provided by the manufacturer datasheets:

- open circuit voltage $V_{oc,ref}$ and short circuit current $I_{sc,ref}$ at the standard rating conditions (SRC): irradiance G_{ref} = 1000 W/m^2, cell temperature T_{ref} = 25 °C and average solar spectrum at AM 1.5;
- voltage $V_{mp,ref}$ and current $I_{mp,ref}$ in the MPP at the SRC;
- open circuit voltage temperature coefficient $\mu_{V,oc}$ and short circuit current temperature coefficient $\mu_{I,sc}$;
- number N_{cs} of series connected PV cells;
- the derivative of the *I-V* curve calculated at the maximum power, short circuit and open circuit points.

Because of the presence of current *I* in both terms of transcendent Equation (2), the solution of the five-equation system, which is necessary to calculate the model parameters, cannot be faced by means of exact mathematical methods. For this reason, both numerical calculation techniques and approximate forms of the equations were adopted.

3. Usability of the One-Diode Models

The models proposed by Hadj Arab *et al.* [24], De Soto *et al.* [25], Sera *et al.* [26], Villalva *et al.* [27], Lo Brano *et al.* [29], Seddaoui *et al.* [35], Siddique *et al.* [49], Yetayew *et al.* [52] and Orioli *et al.* [44] were selected in order to assess the effectiveness of the proposed criterion. The models are based on some fundamental equations that, for the first time, Kennerud [84], Phang *et al.* [85] and de Blas *et al.* [23] described even more than 30 years ago. Unfortunately, such early models were not conceived to allow a complete representation of the *I-V* characteristic for values of the solar irradiance and cell temperature different from the SRC.

To assess the usability rating of a procedure, which may be significantly lowered by the difficulties encountered in using it, it is necessary to explore the complete sequence of operative steps that permit to reach the wished results. Some of the analysed procedures evaluate the model parameters on the basis of similar information, but they adopt different simplifying hypotheses to solve the equations and/or do not use the same relations to describe the dependence on the cell temperature and/or the solar irradiance. A synthetic description of the used information, simplifying hypotheses and solving techniques is contained in the following paragraphs; the analytical procedures to calculate the model parameters are minutely described in the appendix.

3.1. Hadj Arab, Chenlo and Benghanem Model (Link 4)

The model Hadj Arab *et al.* [20] uses the following information:

1. short circuit point [$I = I_{sc,ref}$; $V = 0$];
2. open circuit point [$I = 0$; $V = V_{oc,ref}$];
3. derivative of current at the short circuit point [$\partial I / \partial V = -1/R_{sho}$ at $I = I_{sc,ref}$; $V = 0$];
4. derivative of current at the open circuit point [$\partial I / \partial V = -1/R_{so}$ at $I = 0$; $V = V_{oc,ref}$];
5. MPP [$I = I_{mp,ref}$; $V = V_{mp,ref}$];

and assumes the following hypotheses:

$$e^{\frac{V_{oc,ref}}{nT_{ref}}} >> e^{\frac{I_{sc,ref}R_s}{nT_{ref}}} \quad \frac{I_{0,ref}}{nT_{ref}}e^{\frac{V_{oc,ref}}{nT_{ref}}} >> \frac{1}{R_{sh}}$$
$$R_s << R_{sh} \quad \frac{I_{0,ref}}{nT_{ref}}e^{\frac{I_{sc,ref}R_s}{nT_{ref}}} << \frac{1}{R_{sh}} - \frac{1}{R_{sho}-R_s} \tag{3}$$

The model parameters can be calculated using the explicit equations described in the appendix.

3.2. De Soto, Klein and Beckman Model (Link 5)

The model of De Soto *et al.* [25] is based on the following information:

(1)　short circuit point $[I = I_{sc,mrf}; V = 0]$;
(2)　open circuit point $[I = 0; V = V_{oc,ref}]$;
(3)　MPP $[I = I_{mp,ref}; V = V_{mp,ref}]$;
(4)　derivative of power at the MPP $[\partial P / \partial V = 0; V = V_{mp,ref}]$;
(5)　open circuit point with a cell temperature different from the SRC $[I = 0; V = V_{oc}; G = G_{ref}; T \neq T_{ref}]$.

No simplifying hypothesis is assumed. To simultaneously solve the system of five equations described in the appendix, De Soto *et al.* use a non-linear equation solver, such as Engineering Equation Solver (EES) [86]. Laudani *et al.* proposed the use of closed forms to find the parameters of the De Soto *et al.* model [87].

3.3. Sera, Teodorescu and Rodriguez Model (Link 6)

The model proposed by Sera *et al.* [26] calculates the model parameters by means of following information:

(1)　short circuit point $[I = I_{sc,ref}; V = 0]$;
(2)　open circuit point $[I = 0; V = V_{oc,ref}]$;
(3)　MPP $[I = I_{mp,ref}; V = V_{mp,ref}]$;
(4)　derivative of power at the MPP $[\partial P / \partial V = 0; V = V_{mp,ref}]$;
(5)　derivative of current at the short circuit point $[\partial I / \partial V = -1/R_{sho}$ at $I = I_{sc,ref}; V = 0]$.

The following hypotheses are assumed:

$$
\begin{aligned}
&e^{\frac{V_{oc,ref}}{nT_{ref}}} >> 1 \quad e^{\frac{I_{sc,ref}R_s}{nT_{ref}}} >> 1 \quad e^{\frac{V_{mp,ref}+I_{mp,ref}R_s}{nT_{ref}}} >> 1 \\
&e^{\frac{V_{oc,ref}}{nT_{ref}}} >> e^{\frac{I_{sc,ref}R_s}{nT_{ref}}} \quad R_{sh} = R_{sho}
\end{aligned}
\tag{4}
$$

Due to the presence of implicit forms, the equation system is solved with the nine-step procedure described in the appendix.

3.4. Villalva, Gazoli and Filho Model (Link 8)

Villalva *et al.* [27] propose a model based on the following information:

(1)　short circuit point $[I = I_{sc,ref}; V = 0]$;
(2)　open circuit point $[I = 0; V = V_{oc,ref}]$;
(3)　MPP $[I = I_{mp,ref}; V = V_{mp,ref}]$;
(4)　maximum power $[P = P_{mp,ref}]$;
(5)　fixed shape factor $[1 \leqslant a \leqslant 1.5]$.

The following hypotheses are assumed:

$$
e^{\frac{I_{sc,ref}R_s}{nT_{ref}}} \approx 1 \quad \frac{V_{oc,ref}}{R_{sh}} \approx 0
\tag{5}
$$

and the nine-step iterative method described in the appendix is used to calculate the model parameters.

3.5. Lo Brano, Orioli, Ciulla and Di Gangi Model (Link 9)

The model Lo Brano *et al.* [29] uses the following information:

(1)　short circuit point $[I = I_{sc,ref}; V = 0]$;
(2)　open circuit point $[I = 0; V = V_{oc,ref}]$;
(3)　derivative of current at the short circuit point $[\partial I / \partial V = -1/R_{sho}$ at $I = I_{sc,ref}; V = 0]$;

(4)　derivative of current at the open circuit point [$\partial I/\partial V = -1/R_{so}$ at $I = 0$; $V = V_{oc,ref}$];
(5)　MPP [$I = I_{mp,ref}$; $V = V_{mp,ref}$].

The model adopts a modified version of Equation (2):

$$
\begin{aligned}
I(G,T) = \quad & \alpha_G I_L(T) - I_0(\alpha_G, T) \left(e^{\frac{\alpha_G[V+KI(T-T_{ref})]+IR_{s,ref}}{\alpha_G nT}} - 1 \right) \\
& - \frac{\alpha_G[V+KI(T-T_{ref})]+IR_{s,ref}}{R_{sh,ref}}
\end{aligned}
\tag{6}
$$

where $\alpha_G = G/G_{ref}$ denotes the ratio between the generic solar irradiance and the solar irradiance at the SRC and K is a thermal correction factor similar to the curve correction factor described by the IEC891. Obviously, at the SRC, it is $\alpha_G = 1$, $T = T_{ref}$ and Equation (6) becomes equal to the traditional five-parameter Equation (2). $R_{s,ref}$ and $R_{sh,ref}$ are the series and shunt resistances at the SRC, respectively. Due to presence of term α_G in Equation (6), it is also assumed that the series and shunt resistance are inversely affected by the solar irradiance:

$$
R_s(G) = \frac{R_{s,ref}}{\alpha_G} \qquad R_{sh}(G) = \frac{R_{sh,ref}}{\alpha_G}
\tag{7}
$$

No simplifying hypothesis is assumed and the model parameters are calculated by means of the numerical iterative procedure, based on ten steps, described in the appendix.

3.6. Seddaoui, Rahmani, Kessal and Chauder Model (Link 10)

The Seddaoui *et al.* model [35] is based on the following information:

(1)　short circuit point [$I = I_{sc,ref}$; $V = 0$];
(2)　open circuit point [$I = 0$; $V = V_{oc,ref}$];
(3)　derivative of current at the short circuit point [$\partial I/\partial V = -1/R_{sho}$ at $I = I_{sc,ref}$; $V = 0$];
(4)　derivative of current at the open circuit point [$\partial I/\partial V = -1/R_{so}$ at $I = 0$; $V = V_{oc,ref}$];
(5)　MPP [$I = I_{mp,ref}$; $V = V_{mp,ref}$].

The following hypotheses, also adopted by Phang *et al.* and Hadj Arab *et al.*, are assumed:

$$
\begin{aligned}
& e^{\frac{V_{oc,ref}}{nT_{ref}}} >> e^{\frac{I_{sc,ref}R_s}{nT_{ref}}} \qquad \frac{I_{0,ref}}{nT_{ref}} e^{\frac{V_{oc,ref}}{nT_{ref}}} >> \frac{1}{R_{sh}} \\
& R_s << R_{sh} \qquad \frac{I_{0,ref}}{nT_{ref}} e^{\frac{I_{sc,ref}R_s}{nT_{ref}}} << \frac{1}{R_{sh}} - \frac{1}{R_{sho}-R_s}
\end{aligned}
\tag{8}
$$

The main difference with the Hadj Arab *et al.* model consists in a different way to calculate the *I-V* characteristics for conditions far from the SRC. The model parameters are calculated using the explicit equations described in the appendix.

3.7. Siddique, Xu and De Doncker Model (Link 11)

Siddique *et al.* [49] present a model that uses the following information:

(1)　short circuit point [$I = I_{sc,ref}$; $V = 0$];
(2)　open circuit point [$I = 0$; $V = V_{oc,ref}$];
(3)　MPP [$I = I_{mp,ref}$; $V = V_{mp,ref}$];
(4)　derivative of power at the MPP [$\partial P/\partial V = 0$ at $I = I_{mp,ref}$; $V = V_{mp,ref}$];
(5)　maximum power [$P = P_{mp,ref}$].

No simplifying hypothesis is used and the model parameters are calculated solving some implicit equations by means of the iterative procedure based on twelve steps described in the appendix.

3.8. Yetayew and Jyothsna Model (Link 12)

Yetayew *et al*. [52] propose a model based on the following information:

(1) short circuit point [$I = I_{sc,ref}$; $V = 0$];
(2) open circuit point [$I = 0$; $V = V_{oc,ref}$];
(3) MPP [$I = I_{mp,ref}$; $V = V_{mp,ref}$];
(4) 4th point A at the SRC [$I = I_A$; $V = V_A$ with $0 < V_A < V_{mp,ref}$];
(5) 5th point B at the SRC [$I = I_B$; $V = V_B$ with $V_{mp,ref} < V_B < V_{oc,ref}$].

No simplifying hypothesis is assumed and the equation system described in the appendix is solved by means of the Newton-Raphson method. It is known [88] that the Newton-Raphson technique may result instable because of the wide range of variation of the model parameters. To overcome such a difficulty, the definition of initial values of the model parameters, which should differ from the correct values less than an order of magnitude, is required. Such a task, which is not easy, may make difficult to use the Newton-Raphson method.

3.9. Orioli and Di Gangi Model (Link 13)

The model proposed by Orioli *et al*. [44] adopts the following information:

(1) short circuit point [$I = I_{sc,ref}$; $V = 0$];
(2) open circuit point [$I = 0$; $V = V_{oc,ref}$];
(3) derivative of current at the short circuit point [$\partial I / \partial V = -1/R_{sho}$ at $I = I_{sc,ref}$; $V = 0$];
(4) derivative of current at the open circuit point [$\partial I / \partial V = -1/R_{so}$ at $I = 0$; $V = V_{oc,ref}$];
(5) MPP [$I = I_{mp,ref}$; $V = V_{mp,ref}$].

and assumes the following hypotheses:

$$e^{\frac{I_{sc,ref}R_{s,ref}}{nT_{ref}}} \approx 1 \quad R_{s,ref} << R_{sh,ref} \quad \frac{I_{0,ref}}{nT_{ref}}e^{\frac{I_{sc,ref}R_{s,ref}}{nT_{ref}}} << \frac{1}{R_{sh,ref}} \tag{9}$$

$$e^{\frac{V_{mp,ref}+I_{mp,ref}R_{s,ref}}{nT_{ref}}} >> 1 \quad e^{\frac{V_{oc,ref}}{nT_{ref}}} >> 1 \tag{10}$$

To calculate the model parameters, the equations, which are based on the modified form used by Lo Brano *et al*., are solved using the seven-step iterative procedure described in the appendix.

3.10. Features Affecting the Model Usability

In order to better appreciate the analogies and differences between the various models, the sets of used information, hypotheses and solving techniques, on which the analysed procedures are based, are summarised in in Table 1.

The set of information used by a one-diode model may affect the usability rating of its analytical procedure. Actually, many performance data can be easily found, because they are always listed in tabular form in the PV module datasheets, whereas some data can be extracted only if a complete set of *I-V* curves is provided by the manufacturers. Also, the required mathematical tools, which include simple algorithms, iterative routines, mathematical methods or dedicated computer software, may have a significant impact on the procedure usability.

Table 1. Summary of the information and solving techniques used by the one-diode models.

MODEL	Information Used for Calculation										Solving Techniques	
	SCP	OCP	MPP	DSCP	DOCP	DMPP	OCP *	Max. Power	Fixed *a*	Points 4th 5th	Simplifying Hypotheses	Mathematical Tools
Hadj Arab *et al*.	X	X	X	X	X						X	SC
De Soto *et al*.	X	X	X			X	X					NES
Sera *et al*.	X	X	X	X		X					X	IP
Villalva *et al*.	X	X	X					X	X		X	IP
Lo Brano *et al*.	X	X	X	X	X							IP
Seddaoui *et al*.	X	X	X	X	X						X	SC
Siddique *et al*.	X	X	X			X		X				IP
Yetayew *et al*.	X	X	X							X		NRM
Orioli *et al*.	X	X	X	X	X						X	IP

Notes: SCP: Short Circuit Point; OCP: Open Circuit Point; MPP: Maximum Power Point; DSCP: Derivative of *I* at the SCP; DOCP: Derivative of *I* at the OCP; DMPP: Derivative of power at the MPP; OCP *: OCP at condition $\neq$ SRC; SC: Simple Calculation; NES: Non-linear Equation Solver; IP: Iterative Procedure; NRM: Newton-Raphson Method.

4. Accuracy of the One-Diode Models

In order to assess the accuracy of the proposed procedures, a comparison between the tested one-diode models was made using the *I-V* characteristics extracted from manufacturer datasheets by reading the coordinates of a large number of points on each curve. For the sake of brevity, only two PV modules, based on different production technologies, were considered. Obviously, because the results are strongly affected by the particular shape of the considered *I-V* characteristics, a more reliable assessment may require the use of a greater number of PV modules. Actually, the aim of this accuracy assessment is not ranking the best or the worst among the analysed models, but only reckoning the range of predictable precision in order to calibrate the proposed criterion. The data of the simulated PV modules are listed in Table 2.

Table 2. Performance data of the simulated PV panels.

PANEL	Type	N_{cs}	$V_{oc,ref}$ [V]	$I_{sc,ref}$ [A]	$V_{mp,ref}$ [V]	$I_{mp,ref}$ [A]	$\mu_{V,oc}$ [V/°C]	$\mu_{I,sc}$ [A/°C]	R_{so} [Ω]	R_{sho} [Ω]
Kyocera KD245GH-4FB2	Poly	60	36.90	8.91	29.80	8.23	-1.33×10^{-1}	5.35×10^{-3}	0.493	120.5
Sanyo HIT-240 HDE4	HIT	60	43.60	7.37	35.50	6.77	-1.09×10^{-1}	2.21×10^{-3}	0.873	3204.6

The Lo Brano *et al*. and the Orioli *et al*. models also use the open voltage at $G = 200$ W/m² and $T = 25$ °C, which are 34.40 V and 40.61 V per the Kyocera and the Sanyo PV modules, respectively. To calculate parameter *K*, these models use the values of voltage and current at the MPP for $G = 1000$ W/m² and $T = 75$ °C, which are 22.50 V and 8.35 A, for the Kyocera PV panel, and 28.89 V and 7.13 A, for the Sanyo PV module. In order to get a reliable comparison between the calculated and the experimental data, numerous points were extracted from the *I-V* characteristics issued by the manufacturer, considering both the constant solar irradiance and the constant cell temperature curves. To calculate R_{sho} and R_{so}, the reciprocal of slopes of the *I-V* curve in correspondence of the short circuit and open circuit points were extracted from the issued *I-V* characteristics following the graphical procedure described in [44]. Table 3 and Table 4 list the values of the parameters evaluated with the analysed models.

The values of Table 3 and Table 4 were used to calculate the *I-V* characteristics of the selected PV panels. In Figure 4, Figure 5, Figure 6, Figure 7, Figure 8 and Figure 9 the *I-V* curves evaluated at $T = 25$ °C with the models of Hadj Arab *et al*., De Soto *et al*., Sera *et al*., Villalva *et al*., Lo Brano *et al*., Seddaoui *et al*., Siddique *et al*., Yetayew *et al*. and Orioli *et al*. are compared with the characteristics issued by manufacturers.

Table 3. Model parameters of Kyocera KD245GH-4FB2 at the SRC.

Model	$I_{L,ref}$ [A]	$I_{0,ref}$ [A]	n [V/K]	R_s [Ω]	R_{sh} [Ω]	K [Ω/°C]
Hadj Arab *et al.*	8.9336	1.6881×10^{-10}	5.0199×10^{-3}	0.3189	120.4800	-
De Soto *et al.*	8.9270	1.5328×10^{-9}	5.5111×10^{-3}	0.2854	149.2274	-
Sera *et al.*	8.9126	3.9061×10^{-7}	7.3079×10^{-3}	0.1615	548.4865	-
Villalva *et al.*	8.9157	8.9791×10^{-8}	6.7215×10^{-3}	0.2000	311.0804	-
Lo Brano *et al.*	8.9337	1.6143×10^{-10}	5.0103×10^{-3}	0.3200	120.1600	8.6230×10^{-4}
Seddaoui *et al.*	8.9336	1.6881×10^{-10}	5.0199×10^{-3}	0.3189	120.4800	-
Siddique *et al.*	8.9100	5.6501×10^{-5}	2.7675×10^{-4}	0.1181	$3.7815 \cdot 10^6$	-
Yetayew *et al.*	8.9384	2.0052×10^{-11}	4.6206×10^{-3}	0.3552	111.6164	-
Orioli *et al.*	8.9100	1.6965×10^{-9}	5.5369×10^{-3}	0.2722	142.8660	9.7323×10^{-4}

Table 4. Model parameters of Sanyo HIT-240 HDE4 at the SRC.

MODEL	$I_{L,ref}$ [A]	$I_{0,ref}$ [A]	n [V/K]	R_s [Ω]	R_{sh} [Ω]	K [Ω/°C]
Hadj Arab *et al.*	7.3716	9.6843×10^{-14}	4.5754×10^{-3}	0.6877	3204.6400	-
De Soto *et al.*	7.3958	1.8862×10^{-11}	5.4876×10^{-3}	0.4555	130.0439	-
Sera *et al.*	7.3721	7.9253×10^{-7}	9.1206×10^{-3}	0.1420	488.0935	-
Villalva *et al.*	7.3842	2.6233×10^{-9}	6.7215×10^{-3}	0.3300	171.2005	-
Lo Brano *et al.*	7.3716	9.6380×10^{-14}	4.5747×10^{-3}	0.6877	3203.9523	-1.600×10^3
Seddaoui *et al.*	7.3716	9.6843×10^{-14}	4.5754×10^{-3}	0.6877	3204.6400	-
Siddique *et al.*	7.3700	5.3195×10^{-6}	7.1635×10^{-3}	0.0542	$2.2747 \cdot 10^7$	-
Yetayew *et al.*	7.3716	1.5551×10^{-14}	4.3277×10^{-3}	0.7152	3212.5368	-
Orioli *et al.*	7.3700	3.6671×10^{-19}	3.2907×10^{-3}	0.8200	736.4149	-6.4618×10^4
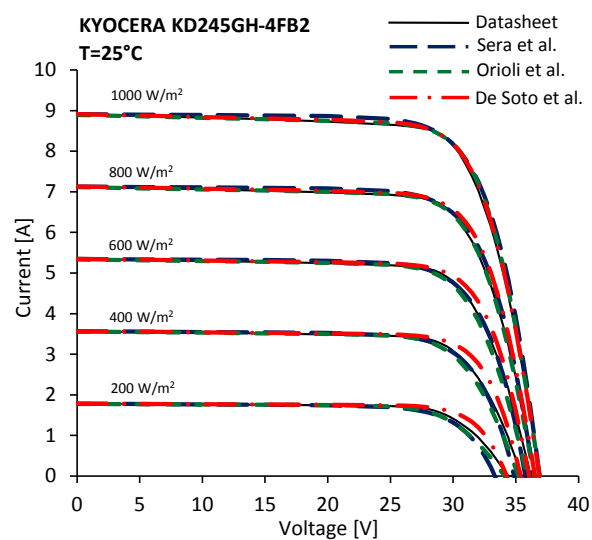
Figure 4. Comparison between the issued *I-V* characteristics of Kyocera KD245GH-4FB2 at *T* = 25 °C and the characteristics calculated by means of the Sera *et al.*, the Orioli *et al.* and the De Soto *et al.* models.

Figure 5. Comparison between the issued *I-V* characteristics of Kyocera KD245GH-4FB2 at *T* = 25 °C and the characteristics calculated by means of the Villalva *et al.*, the Yetayew *et al.* and the Seddaoui *et al.* models.

Figure 6. Comparison between the issued *I-V* characteristics of Kyocera KD245GH-4FB2 at *T* = 25 °C and the characteristics calculated by means of the Lo Brano *et al.*, the Siddique *et al.* and the Hadj Arab *et al.* models.

Figure 7. Comparison between the issued *I-V* characteristics of Sanyo HIT-240 HDE4 at *T* = 25 °C and the characteristics calculated by means of the Sera *et al.*, the Orioli *et al.* and the De Soto *et al.* models.

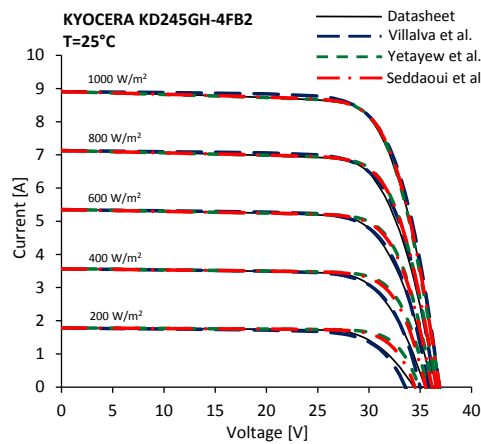**Figure 8.** Comparison between the issued *I-V* characteristics of Sanyo HIT-240 HDE4 at *T* = 25 °C and the characteristics calculated by means of the Villalva *et al.*, the Yetayew *et al.* and the Seddaoui *et al.* models.
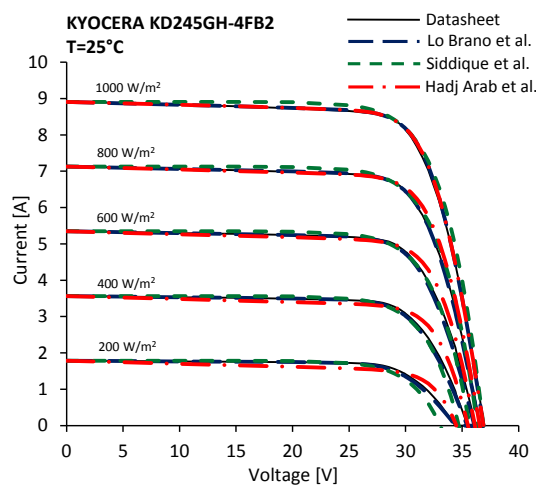
Figure 9. Comparison between the issued *I-V* characteristics of Sanyo HIT-240 HDE4 at *T* = 25 °C and the characteristics calculated by means of the Lo Brano *et al.*, the Siddique *et al.* and the Hadj Arab *et al.* models.

Because the Hadj Arab *et al.* and the Seddaoui *et al.* are based on the same information, it is not surprising that the *I-V* curves at the SRC resulted quite similar. Conversely, significant differences are expected for values of solar irradiance and temperature different from the SRC. Figures 10–15 depict the *I-V* curves evaluated at *G* = 1000 W/m^2 and the characteristics issued by manufacturers.

Figure 10. Comparison between the issued *I-V* characteristics of Kyocera KD245GH-4FB2 at $G = 1000 \text{ W/m}^2$ and the characteristics calculated by means of the Sera *et al.*, the Orioli *et al.* and the De Soto *et al.* models.

Figure 11. Comparison between the issued *I-V* characteristics of Kyocera KD245GH-4FB2 at $G = 1000 \text{ W/m}^2$ and the characteristics calculated by means of the Villalva *et al.*, the Yetayew *et al.* and the Seddaoui *et al.* models.
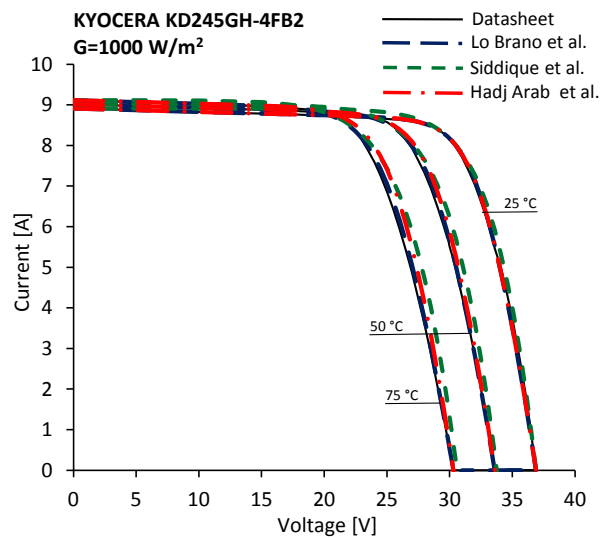
Figure 12. Comparison between the issued *I-V* characteristics of Kyocera KD245GH-4FB2 at $G = 1000 \text{ W/m}^2$ and the characteristics calculated by means of the Lo Brano *et al.*, the Siddique *et al.* and the Hadj Arab *et al.* models.
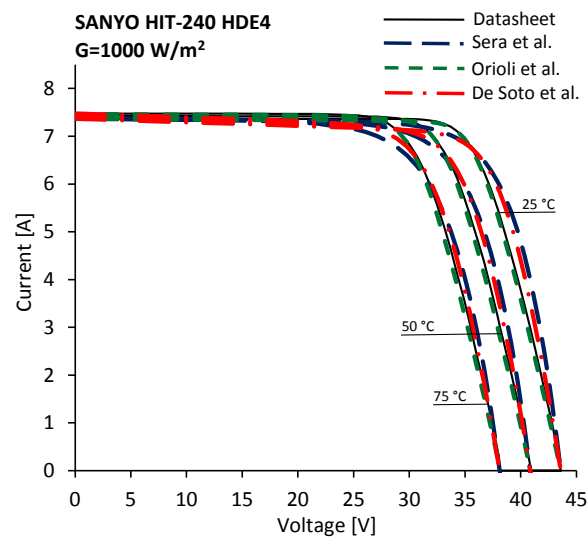
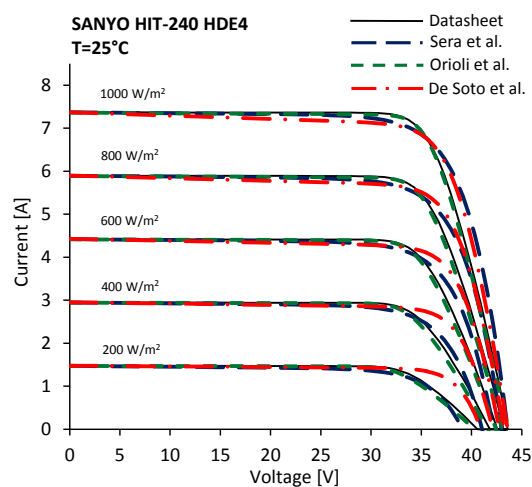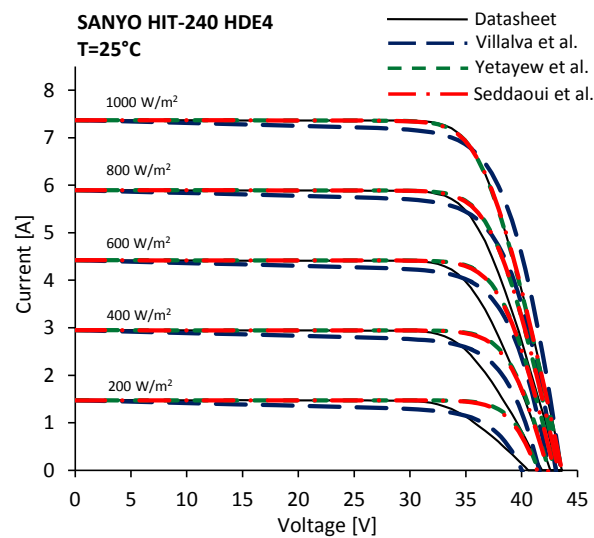**Figure 13.** Comparison between the issued *I-V* characteristics of Sanyo HIT-240 HDE4 at $G = 1000 \text{ W/m}^2$ and the characteristics calculated by means of the Sera *et al.*, the Orioli *et al.* and the De Soto *et al.* models.
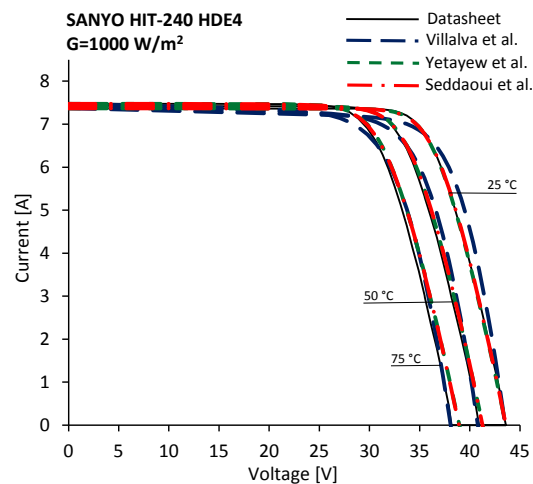
Figure 14. Comparison between the issued *I-V* characteristics of Sanyo HIT-240 HDE4 at $G = 1000 \, \text{W/m}^2$ and the characteristics calculated by means of the Villalva *et al.*, the Yetayew *et al.* and the Seddaoui *et al.* models.

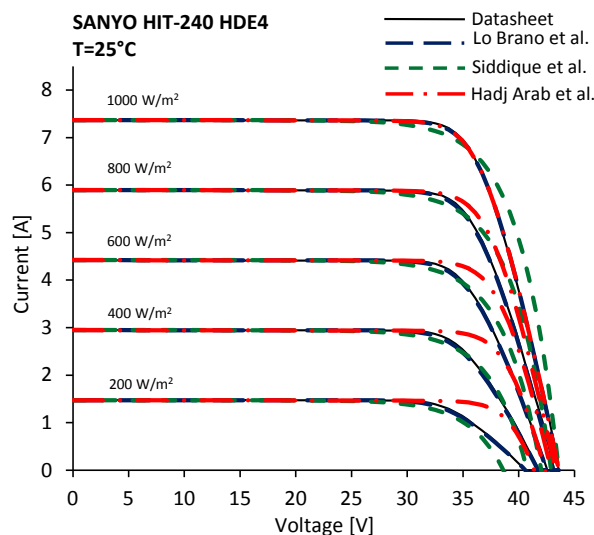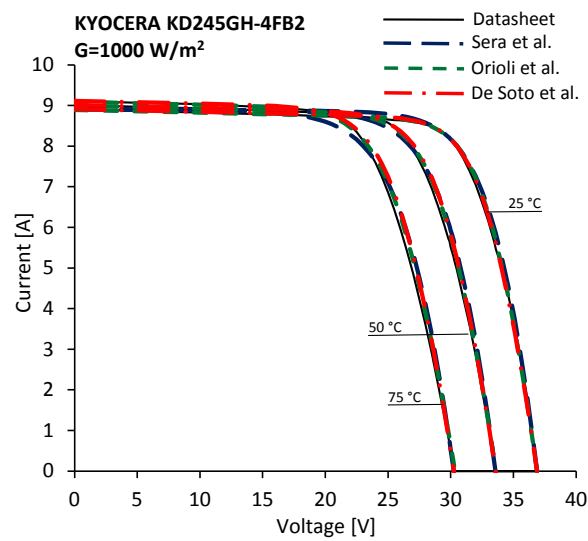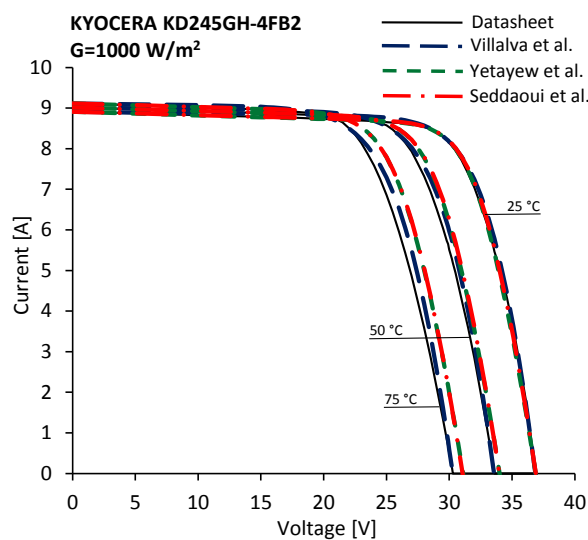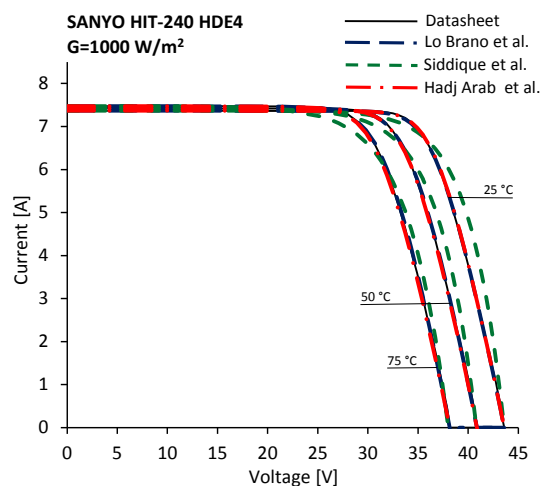**Figure 15.** Comparison between the issued *I-V* characteristics of Sanyo HIT-240 HDE4 at $G = 1000 \, \text{W/m}^2$ and the characteristics calculated by means of the Lo Brano *et al.*, the Siddique *et al.* and the Hadj Arab *et al.* models.

It can be generally observed in Figures 4–15 that most of the models result less accurate for values of voltage greater than the MPP voltage. Moreover, it can be inferred that the one-diode models are more precise if they are used to evaluate the *I-V* characteristics of the Kyocera PV panel. This occurrence may be due to the different shape of the *I-V* curves used to compare the analysed models. It can be also observed that models that use similar values of the parameters listed in Table 3 and Table 4 yield different *I-V* curves for values of the solar irradiance and the cell temperature far from the SRC because different approaches were adopted to describe the effects of the solar irradiance and cell temperature. To quantify the accuracy of the analysed models, the mean absolute difference (MAD) for current and power was calculated with the following expressions:

$$\text{MAD}(I) = \frac{1}{N} \sum_{j=1}^{N} \left| I_{calc,j} - I_{iss,j} \right| \tag{11}$$

$$\text{MAD}(P) = \frac{1}{N} \sum_{j=1}^{N} \left| V_{iss,j} I_{calc,j} - V_{iss,j} I_{iss,j} \right| \tag{12}$$

in which $V_{iss,j}$ and $I_{iss,j}$ are the voltage and current of the *j*-th point extracted from the *I-V* characteristics issued by manufacturers, $I_{calc,j}$ is the value of the current calculated in correspondence of $V_{iss,j}$ and N is the number of extracted points. Moreover, in order to assess the range of dispersion of the results, also the maximum difference (MD) for current and power was evaluated using the following relations:

$$\text{MD}(I) = \text{MAX} \left[I_{calc,j} - I_{iss,j} \right] \tag{13}$$

$$\text{MD}(P) = \text{MAX} \left[V_{iss,j} I_{calc,j} - V_{iss,j} I_{iss,j} \right] \tag{14}$$

Tables 5 and 6 list the MAD(*I*)s and MAD(*P*)s for the Kyocera KD245GH-4FB2 and Sanyo HIT-240 HDE4 PV panels.

Table 5. Mean absolute current and power differences between the calculated and the issued *I–V* characteristics at temperature $T = 25\,^{\circ}\text{C}$.

PV Panel	Mad	Irradiance [W/m^2]				
		200	**400**	**600**	**800**	**1000**
Kyocera KD245GH-4FB2	Current [A]					
	Hadj Arab *et al.* model	0.110	0.153	0.130	0.111	0.042
	De Soto *et al.* model	0.101	0.149	0.132	0.124	0.052
	Sera *et al.* model	0.094	0.065	0.057	0.092	0.136
	Villalva *et al.* model	0.077	0.054	0.050	0.089	0.104
	Lo Brano *et al.* model	0.041	0.059	0.082	0.033	0.042
	Seddaoui *et al.* model	0.138	0.187	0.156	0.131	0.042
	Siddique *et al.* model	0.137	0.123	0.087	0.094	0.166
	Yetayew *et al.* model	0.209	0.253	0.192	0.136	0.051
	Orioli *et al.* model	0.076	0.107	0.115	0.042	0.064
	Power [W]					
	Hadj Arab *et al.* model	3.138	4.718	4.077	3.595	1.350
	De Soto *et al.* model	3.103	4.681	4.166	3.948	1.608
	Sera *et al.* model	2.851	2.075	1.772	2.869	4.257
	Villalva *et al.* model	2.299	1.769	1.607	2.805	3.192
	Lo Brano *et al.* model	1.246	1.870	2.698	1.074	1.356
	Seddaoui *et al.* model	4.320	5.977	5.006	4.216	1.350
	Siddique *et al.* model	4.173	3.901	2.698	2.881	5.229
	Yetayew *et al.* model	6.625	8.123	6.184	4.387	6.625
	Orioli *et al.* model	2.313	3.421	3.738	1.366	2.044
Sanyo HIT-240 HDE4	Current [A]					
	Hadj Arab *et al.* model	0.230	0.324	0.323	0.186	0.021
	De Soto *et al.* model	0.173	0.286	0.333	0.307	0.242
	Sera *et al.* model	0.072	0.100	0.174	0.234	0.321
	Villalva *et al.* model	0.109	0.194	0.266	0.269	0.267
	Lo Brano *et al.* model	0.015	0.028	0.022	0.041	0.021
	Seddaoui *et al.* model	0.235	0.327	0.326	0.187	0.021
	Siddique *et al.* model	0.102	0.074	0.136	0.212	0.337
	Yetayew *et al.* model	0.251	0.346	0.340	0.190	0.024
	Orioli *et al.* model	0.056	0.079	0.075	0.100	0.078
	Power [W]					
	Hadj Arab *et al.* model	8.656	12.436	12.518	7.226	0.828
	De Soto *et al.* model	6.362	10.750	12.598	11.382	8.686
	Sera *et al.* model	2.303	3.465	6.428	8.855	12.496
	Villalva *et al.* model	3.303	6.735	9.664	9.858	9.846
	Lo Brano *et al.* model	0.487	1.011	0.794	1.601	0.830
	Seddaoui *et al.* model	8.813	12.551	12.593	7.256	0.828
	Siddique *et al.* model	3.591	2.646	5.060	8.179	13.321
	Yetayew *et al.* model	9.427	13.281	13.125	7.350	0.963
	Orioli *et al.* model	1.963	2.913	2.805	3.799	2.952

Table 6. Mean absolute current and power differences between the calculated andthe issued *I–V* characteristics at irradiance $G = 1000 \, \text{W/m}^2$.

PV Panel	Mad	Temperature [°C]		
		25	**50**	**75**
Kyocera KD245GH-4FB2	Current [A]			
	Hadj Arab *et al.* model	0.042	0.125	0.200
	De Soto *et al.* model	0.052	0.116	0.136
	Sera *et al.* model	0.136	0.150	0.212
	Villalva *et al.* model	0.104	0.178	0.191
	Lo Brano *et al.* model	0.042	0.048	0.063
	Seddaoui *et al.* model	0.042	0.314	0.655
	Siddique *et al.* model	0.166	0.308	0.413
	Yetayew *et al.* model	0.051	0.287	0.651
	Orioli *et al.* model	0.064	0.088	0.113
	Power [W]			
	Hadj Arab *et al.* model	1.350	3.628	5.215
	De Soto *et al.* model	1.608	3.269	3.481
	Sera *et al.* model	4.257	4.298	4.858
	Villalva *et al.* model	3.192	4.960	4.943
	Lo Brano *et al.* model	1.356	1.333	1.611
	Seddaoui *et al.* model	1.350	9.453	18.222
	Siddique *et al.* model	5.229	8.807	11.297
	Yetayew *et al.* model	6.625	8.680	18.140
	Orioli *et al.* model	2.044	2.526	2.984
Sanyo HIT-240 HDE4	Current [A]			
	Hadj Arab *et al.* model	0.021	0.035	0.066
	De Soto *et al.* model	0.242	0.205	0.151
	Sera *et al.* model	0.321	0.292	0.273
	Villalva *et al.* model	0.267	0.236	0.195
	Lo Brano *et al.* model	0.021	0.029	0.034
	Seddaoui *et al.* model	0.021	0.114	0.247
	Siddique *et al.* model	0.337	0.283	0.231
	Yetayew *et al.* model	0.024	0.107	0.252
	Orioli *et al.* model	0.078	0.102	0.117
	Power [W]			
	Hadj Arab *et al.* model	0.828	1.292	2.257
	De Soto *et al.* model	8.686	6.729	4.506
	Sera *et al.* model	12.496	9.984	8.167
	Villalva *et al.* model	9.846	8.019	6.132
	Lo Brano *et al.* model	0.830	1.049	1.142
	Seddaoui *et al.* model	0.828	4.270	8.799
	Siddique *et al.* model	13.321	10.170	7.550
	Yetayew *et al.* model	0.963	4.042	8.991
	Orioli *et al.* model	2.952	3.623	3.951

Considering the solar irradiance variation, if the Hadj Arab *et al.*, the Villalva *et al.*, the Lo Brano *et al.* and the Seddaoui *et al.* models are used for the Kyocera PV panel, MAD(*I*)s ranging

from 0.041 A to 0.054 A can be obtained. In the same conditions, the MAD(*P*)s vary from 1.074 W to 1.769 W. For the Sanyo PV module, the smallest MAD(*I*)s, which occur when the Hadj Arab *et al.*, the Lo Brano *et al.* and the Seddaoui *et al.* models are used, vary between 0.015 A and 0.041 A. The smallest MAD(*P*)s derived from the same models. These differences vary between 0.487 W and 1.601 W. The greatest MAD(*I*)s for the Kyocera PV panel, which are calculated with the Siddique *et al.* and the Yetayew *et al.* models, vary from 0.136 A to 0.253 A. The Yetayew *et al.* model yields the greatest MAD(*P*)s, which range from 4.387 W to 8.123 W. For the Sanyo PV module, the greatest MAD(*I*)s are noted for the De Soto *et al.*, the Siddique *et al.* and the Yetayew *et al.* models. These differences are contained in the range from 0.251 A to 0.346 A. The greatest MAD(*P*)s, which belong to the same models, vary from 9.427 W to 13.321 W.

At constant solar irradiance, if the Hadj Arab *et al.*, the Lo Brano *et al.* and the Seddaoui *et al.* models are used for the Kyocera PV panel, MAD(*I*)s ranging from 0.042 A to 0.063 A can be observed. In the same conditions, the MAD(*P*)s vary from 1.333 W to 1.611 W. For the Sanyo PV module, the smallest MAD(*I*)s, which are obtained from the Hadj Arab *et al.*, the Lo Brano *et al.* and the Seddaoui *et al.* models, vary between 0.021 A and 0.034 A. The smallest mean power differences are obtained from the same models. These differences vary between 0.828 W and 1.142 W. For the Kyocera PV module, the greatest MAD(*I*)s are generated by the Seddaoui *et al.* and the Siddique *et al.* models. These differences are contained in the range from 0.166 A to 0.655 A. The greatest MAD(*P*)s, which are obtained from the Seddaoui *et al.* and the Yetayew *et al.* models, vary between 6.625 W and 18.222 W. The greatest MAD(*I*)s for the Sanyo PV panel, which are obtained from the Sera *et al.* and the Siddique *et al.* models, vary from 0.273 A to 0.337 A. The Siddique *et al.* and the Yetayew *et al.* models yield the greatest MAD(*P*)s, which range from 8.991 W to 13.321 W of the issued rated maximum power. In Tables 7 and 8 the values of MD(*I*) and MD(*P*) for the analysed panels, calculated considering the *I-V* curves at a constant cell temperature of 25 °C, are listed.

Considering the *I-V* curves at constant temperature for the Kyocera PV panel, the Lo Brano *et al.* model seems to be the most accurate; the MD(*I*)s vary from −0.257 A to 0.132 A. The greatest current differences, which are contained in the range −0.574 A to 0.636 A, are observed for the Siddique *et al.* and the Yetayew *et al.* models. The smallest MD(*I*)s are obtained for the Sanyo PV module from the Hadj Arab *et al.*, the Lo Brano *et al.* and the Seddaoui *et al.* models; these differences are in the range −0.040 A to −0.147 A. The greatest inaccuracies derive from the de Soto *et al.*, the Siddique *et al.* and the Yetayew *et al.* models. For these models differences varying between 0.724 A and 1.125 A were calculated. Table 9 and Table 10 list the MD(*I*)s calculated for Kyocera KD245GH-4FB2 and Sanyo HIT-240 HDE4 PV panels at a constant solar irradiance of 1000 W/m^2.

Table 7. Maximum current differences between the calculated and the issued *I-V* characteristics of Kyocera KD245GH-4FB2, at temperature *T* = 25 °C.

Parameters At The Maximum Difference Points		Irradiance [W/m²]				
		200	**400**	**600**	**800**	**1000**
Hadj Arab *et al.* model	Voltage [V]	33.0	33.0	33.0	32.5	32.5
	Issued Current [A]	0.603	1.896	3.335	5.093	6.596
	Calculated Current [A]	0.849	2.306	3.708	5.428	6.735
	Difference [A]	0.246	0.410	0.373	0.335	0.139
De Soto *et al.* model	Voltage [V]	32.0	32.5	33.0	32.5	32.5
	Issued Current [A]	0.948	2.165	3.335	5.093	6.596
	Calculated Current [A]	1.200	2.553	3.686	5.428	6.765
	Difference [A]	0.252	0.388	0.351	0.335	0.169
Sera *et al.* model	Voltage [V]	33.0	34.5	35.5	33.5	34.5
	Issued Current [A]	0.603	0.843	0.891	4.224	4.305
	Calculated Current [A]	0.221	0.460	0.466	4.479	4.687
	Difference [A]	−0.382	−0.383	−0.425	0.255	0.382
Villalva *et al.* model	Voltage [V]	33.5	35.0	35.5	33.5	34.0
	Issued Current [A]	0.394	0.429	0.891	4.224	4.992
	Calculated Current [A]	0.037	0.001	0.553	4.471	5.259
	Difference [A]	−0.357	−0.428	−0.338	0.247	0.267
Lo Brano *et al.* model	Voltage [V]	32.0	33.5	34.4	35.0	32.5
	Issued Current [A]	0.948	1.591	2.151	2.441	6.596
	Calculated Current [A]	0.860	1.443	1.894	2.325	6.728
	Difference [A]	−0.088	−0.148	−0.257	−0.116	0.132
Seddaoui *et al.* model	Voltage [V]	32.5	33.0	33.0	32.5	32.5
	Issued Current [A]	0.780	1.896	3.335	5.093	6.596
	Calculated Current [A]	1.145	2.395	3.765	5.460	6.735
	Difference [A]	0.366	0.499	0.430	0.367	0.139
Siddique *et al.* model	Voltage [V]	33.0	34.5	35.5	36.2	34.5
	Issued Current [A]	0.603	0.843	0.891	0.655	4.305
	Calculated Current [A]	0.045	0.267	0.317	0.365	4.786
	Difference [A]	−0.558	−0.576	−0.574	−0.290	0.481
Yetayew *et al.* model	Voltage [V]	33.0	33.0	33.0	32.5	36.2
	Issued Current [A]	0.603	1.896	3.335	5.093	1.500
	Calculated Current [A]	1.144	2.532	3.844	5.471	1.324
	Difference [A]	0.541	0.636	0.509	0.378	−0.176
Orioli *et al.* model	Voltage [V]	33.0	34.4	35.5	36.2	32.5
	Issued Current [A]	0.603	0.945	0.891	0.655	6.596
	Calculated Current [A]	0.450	0.674	0.536	0.444	6.816
	Difference [A]	−0.153	−0.271	−0.355	−0.211	0.220

Table 8. Maximum current differences between the calculated and the issued *I-V* characteristics of Sanyo HIT-240 HDE4, at temperature $T = 25\ ^{\circ}$C.

Parameters At The Maximum Difference Points		Irradiance [W/m^2]				
		200	**400**	**600**	**800**	**1000**
Hadj Arab *et al.* model	Voltage [V]	38.5	39.1	39.1	39.1	42.7
	Issued Current [A]	0.471	1.187	2.171	3.350	1.070
	Calculated Current [A]	1.147	2.128	3.093	3.903	0.971
	Difference [A]	0.676	0.941	0.922	0.553	−0.099
De Soto *et al.* model	Voltage [V]	38.5	39.1	39.7	39.1	39.7
	Issued Current [A]	0.471	1.187	1.819	3.350	4.018
	Calculated Current [A]	1.000	2.029	2.802	4.191	4.653
	Difference [A]	0.529	0.842	0.983	0.841	0.635
Sera *et al.* model	Voltage [V]	38.5	40.9	39.1	40.3	40.3
	Issued Current [A]	0.471	0.401	2.171	2.458	3.485
	Calculated Current [A]	0.254	0.117	2.722	3.224	4.516
	Difference [A]	−0.217	−0.284	0.551	0.766	1.031
Villalva *et al.* model	Voltage [V]	29.8	38.5	39.1	39.7	39.7
	Issued Current [A]	1.464	1.414	2.171	2.934	4.018
	Calculated Current [A]	1.291	1.922	2.918	3.702	4.791
	Difference [A]	−0.173	0.508	0.747	0.768	0.773
Lo Brano *et al.* model	Voltage [V]	34.9	34.9	34.3	42.1	42.7
	Issued Current [A]	1.144	2.551	4.128	1.010	1.070
	Calculated Current [A]	1.104	2.491	4.080	0.863	0.971
	Difference [A]	−0.040	−0.060	−0.048	−0.147	−0.099
Seddaoui *et al.* model	Voltage [V]	38.5	39.1	39.1	39.1	42.7
	Issued Current [A]	0.471	1.187	2.171	3.350	1.070
	Calculated Current [A]	1.152	2.132	3.095	3.904	0.971
	Difference [A]	0.681	0.945	0.924	0.554	−0.099
Siddique *et al.* model	Voltage [V]	38.5	40.6	39.1	40.3	40.6
	Issued Current [A]	0.471	0.554	2.171	2.458	3.233
	Calculated Current [A]	0.051	0.150	2.613	3.195	4.358
	Difference [A]	−0.420	−0.404	0.442	0.737	1.125
Yetayew *et al.* model	Voltage [V]	38.5	39.1	39.1	39.1	42.7
	Issued Current [A]	0.471	1.187	2.171	3.350	1.070
	Calculated Current [A]	1.195	2.177	3.121	3.896	0.953
	Difference [A]	0.724	0.990	0.950	0.546	−0.117
Orioli *et al.* model	Voltage [V]	37.3	37.3	38.5	39.7	40.9
	Issued Current [A]	0.720	1.865	2.508	2.934	2.923
	Calculated Current [A]	0.600	1.682	2.326	2.682	2.701
	Difference [A]	−0.120	−0.183	−0.182	−0.252	−0.222

Table 9. Maximum current differences between the calculated and the issued *I-V* characteristics of Kyocera KD245GH-4FB2, at irradiance $G = 1000$ W/m^2.

Parameters at the Maximum Difference Points		Temperature [°C]		
		25	**50**	**75**
Hadj Arab *et al.* model	Voltage [V]	32.5	29.5	26.0
	Issued Current [A]	6.596	6.039	5.950
	Calculated Current [A]	6.735	6.421	6.594
	Difference [A]	0.139	0.382	0.644
De Soto *et al.* model	Voltage [V]	32.5	29.5	26.0
	Issued Current [A]	6.596	6.039	5.950
	Calculated Current [A]	6.765	6.362	6.412
	Difference [A]	0.169	0.323	0.462
Sera *et al.* model	Voltage [V]	34.5	31.0	27.5
	Issued Current [A]	4.305	4.278	4.241
	Calculated Current [A]	4.687	4.738	4.778
	Difference [A]	0.382	0.460	0.537
Villalva *et al.* model	Voltage [V]	34.0	31.0	27.5
	Issued Current [A]	4.992	4.278	4.241
	Calculated Current [A]	5.259	4.743	4.886
	Difference [A]	0.267	0.465	0.645
Lo Brano *et al.* model	Voltage [V]	32.5	29.0	26.0
	Issued Current [A]	6.596	6.515	5.950
	Calculated Current [A]	6.728	6.683	6.173
	Difference [A]	0.132	0.168	0.223
Seddaoui *et al.* model	Voltage [V]	32.5	31.0	29.0
	Issued Current [A]	6.596	4.278	2.122
	Calculated Current [A]	6.735	5.063	3.638
	Difference [A]	0.139	0.785	1.516
Siddique *et al.* model	Voltage [V]	34.5	31.0	28.5
	Issued Current [A]	4.305	4.278	2.875
	Calculated Current [A]	4.786	5.111	4.012
	Difference [A]	0.481	0.833	1.137
Yetayew *et al.* model	Voltage [V]	36.2	33.6	29.5
	Issued Current [A]	1.500	0.000	1.326
	Calculated Current [A]	1.324	0.787	2.822
	Difference [A]	−0.176	0.787	1.496
Orioli *et al.* model	Voltage [V]	32.5	29.5	27.5
	Issued Current [A]	6.596	6.039	4.241
	Calculated Current [A]	6.816	6.300	4.562
	Difference [A]	0.220	0.261	0.321

Table 10. Maximum current differences between the calculated and the issued *I-V* characteristics of Sanyo HIT-240 HDE4, at irradiance $G = 1000$ W/m^2.

Parameters at the Maximum Difference Points		Temperature [°C]		
		25	**50**	**75**
Hadj Arab *et al.* model	Voltage [V]	42.7	39.7	37.3
	Issued Current [A]	1.070	1.440	1.120
	Calculated Current [A]	0.971	1.293	0.951
	Difference [A]	−0.099	−0.147	−0.169
De Soto *et al.* model	Voltage [V]	39.7	37.3	34.3
	Issued Current [A]	4.018	3.810	4.100
	Calculated Current [A]	4.653	4.263	4.403
	Difference [A]	0.635	0.453	0.303
Sera *et al.* model	Voltage [V]	40.3	38.2	35.5
	Issued Current [A]	3.485	2.981	2.984
	Calculated Current [A]	4.516	3.789	3.535
	Difference [A]	1.031	0.808	0.551
Villalva *et al.* model	Voltage [V]	39.7	37.3	34.3
	Issued Current [A]	4.018	3.810	4.100
	Calculated Current [A]	4.791	4.409	4.556
	Difference [A]	0.773	0.599	0.456
Lo Brano *et al.* model	Voltage [V]	42.7	40.6	37.9
	Issued Current [A]	1.070	0.455	0.438
	Calculated Current [A]	0.971	0.325	0.293
	Difference [A]	−0.099	−0.130	−0.145
Seddaoui *et al.* model	Voltage [V]	42.7	40.9	38.2
	Issued Current [A]	1.070	0.000	0.000
	Calculated Current [A]	0.971	0.383	0.832
	Difference [A]	−0.099	0.383	0.832
Siddique *et al.* model	Voltage [V]	40.6	38.2	35.5
	Issued Current [A]	3.233	2.981	2.984
	Calculated Current [A]	4.358	3.871	3.542
	Difference [A]	1.125	0.890	0.558
Yetayew *et al.* model	Voltage [V]	42.7	40.9	38.2
	Issued Current [A]	1.070	0.000	0.000
	Calculated Current [A]	0.953	0.396	0.858
	Difference [A]	−0.117	0.396	0.858
Orioli *et al.* model	Voltage [V]	40.9	36.7	34.9
	Issued Current [A]	2.923	4.358	3.589
	Calculated Current [A]	2.701	4.109	3.295
	Difference [A]	−0.222	−0.249	−0.294

The smallest MD(*I*)s for the Kyocera PV module at constant solar irradiance arise from the Lo Brano *et al.* model. Such differences range from 0.132 A to 0.223 A. The greatest inaccuracies are provided by the Seddaoui *et al.* and the Siddique *et al.* models, for which differences varying between 0.481 A and 1.516 A are observed. The Hadj Arab *et al.*, the Lo Brano *et al.* and the Seddaoui *et al.* model seem to be the most accurate for the Sanyo PV panel; the MD(*I*)s vary from −0.099 A to −0.145 A. The

greatest current differences, which are contained in the range 0.858 A to 1.125 A, are observed for the Siddique *et al.* and the Yetayew *et al.* models. Table 11–14 list the MD(*P*)s calculated for the analysed PV modules.

Table 11. Maximum power differences between the calculated and the issued *I-V* characteristics of Kyocera KD245GH-4FB2, at temperature *T* = 25 °C.

Parameters at the Maximum Difference Points		Irradiance [W/m²]				
		200	400	600	800	1000
Hadj Arab *et al.* model	Voltage [V]	33.0	33.5	33.0	32.5	32.5
	Issued Power [W]	19.91	53.31	110.06	165.51	214.37
	Calculated Power [W]	28.02	67.00	122.36	176.41	218.90
	Difference [W]	8.11	13.69	12.30	10.90	4.53
De Soto *et al.* model	Voltage [V]	32.5	33.0	33.0	32.5	32.5
	Issued Power [W]	25.34	62.55	110.06	165.51	214.37
	Calculated Power [W]	33.44	75.23	121.63	176.41	219.88
	Difference [W]	8.10	12.68	11.57	10.90	5.51
Sera *et al.* model	Voltage [V]	33.0	34.5	35.5	34.0	34.5
	Issued Power [W]	19.91	29.07	31.65	125.37	148.52
	Calculated Power [W]	7.29	15.85	16.56	133.90	161.71
	Difference [W]	−12.62	−13.22	−15.09	8.53	13.19
Villalva *et al.* model	Voltage [V]	33.5	35.0	35.5	33.5	34.0
	Issued Power [W]	13.20	15.00	31.65	141.51	169.73
	Calculated Power [W]	1.24	0.05	19.62	149.76	178.81
	Difference [W]	−11.96	−14.95	−12.03	8.25	9.08
Lo Brano *et al.* model	Voltage [V]	32.0	33.5	34.4	35.0	36.2
	Issued Power [W]	30.34	53.31	74.00	85.42	54.30
	Calculated Power [W]	27.52	48.33	65.17	81.38	49.86
	Difference [W]	−2.82	−4.98	−8.83	−4.04	-4.44
Seddaoui *et al.* model	Voltage [V]	32.5	33.0	33.0	32.5	32.5
	Issued Power [W]	25.34	62.55	110.06	165.51	214.37
	Calculated Power [W]	37.23	79.04	124.26	177.43	218.90
	Difference [W]	11.89	16.49	14.20	11.92	4.53
Siddique *et al.* model	Voltage [V]	33.0	34.5	35.5	36.2	34.5
	Issued Power [W]	19.91	29.07	31.65	23.70	148.52
	Calculated Power [W]	1.49	9.23	11.25	13.21	165.12
	Difference [W]	−18.42	−19.84	−20.40	−10.49	16.60
Yetayew *et al.* model	Voltage [V]	33.0	33.5	33.0	32.5	32.5
	Issued Power [W]	13.20	53.31	110.06	165.51	54.30
	Calculated Power [W]	31.20	74.63	126.84	177.79	47.92
	Difference [W]	18.00	21.32	16.78	12.28	−6.38
Orioli *et al.* model	Voltage [V]	33.0	34.4	35.5	36.2	32.5
	Issued Power [W]	19.91	32.52	31.65	23.70	214.37
	Calculated Power [W]	14.85	23.17	19.04	16.09	221.53
	Difference [W]	−5.06	−9.35	−12.61	−7.61	7.16

Table 12. Maximum power differences between the calculated and the issued *I-V* characteristics of Sanyo HIT-240 HDE4, at temperature *T* = 25 °C.

Parameters at the Maximum Difference Points		Irradiance [W/m²]				
		200	**400**	**600**	**800**	**1000**
Hadj Arab *et al.* model	Voltage [V]	39.1	39.1	39.1	39.1	42.7
	Issued Power [W]	13.28	46.44	84.96	131.07	45.73
	Calculated Power [W]	39.34	83.25	121.03	152.70	41.51
	Difference [W]	26.06	36.81	36.07	21.63	−4.22
De Soto *et al.* model	Voltage [V]	38.5	39.1	39.7	39.7	39.7
	Issued Power [W]	18.13	46.44	72.26	116.58	159.62
	Calculated Power [W]	38.53	79.38	111.34	149.71	184.86
	Difference [W]	20.40	32.94	39.08	33.13	25.24
Sera *et al.* model	Voltage [V]	38.5	40.9	39.1	40.3	40.6
	Issued Power [W]	18.13	16.42	84.96	99.14	131.28
	Calculated Power [W]	9.78	4.77	106.49	130.01	173.06
	Difference [W]	−8.35	−11.65	21.53	30.87	41.78
Villalva *et al.* model	Voltage [V]	37.3	38.5	39.7	40.3	39.7
	Issued Power [W]	26.89	54.47	72.26	99.14	159.62
	Calculated Power [W]	33.02	74.04	101.86	129.68	190.36
	Difference [W]	6.13	19.57	29.60	30.54	30.74
Lo Brano *et al.* model	Voltage [V]	34.9	34.9	42.1	42.1	42.7
	Issued Power [W]	39.96	89.08	12.36	42.57	45.73
	Calculated Power [W]	38.55	86.97	10.54	36.38	41.49
	Difference [W]	−1.41	−2.11	−1.82	−6.19	−4.24
Seddaoui *et al.* model	Voltage [V]	38.5	39.1	39.1	39.1	42.7
	Issued Power [W]	18.13	46.44	84.96	131.07	45.73
	Calculated Power [W]	44.39	83.41	121.09	152.74	41.51
	Difference [W]	26.26	36.97	36.13	21.67	−4.22
Siddique *et al.* model	Voltage [V]	38.5	40.6	39.1	40.3	40.6
	Issued Power [W]	18.13	22.48	84.96	99.14	131.28
	Calculated Power [W]	1.96	6.07	102.25	128.85	176.96
	Difference [W]	−16.17	−16.41	17.29	29.71	45.68
Yetayew *et al.* model	Voltage [V]	39.1	39.1	39.1	39.1	42.7
	Issued Power [W]	13.28	46.44	84.96	131.07	45.73
	Calculated Power [W]	41.49	85.18	122.11	152.43	40.73
	Difference [W]	28.21	38.74	37.15	21.36	−5.00
Orioli *et al.* model	Voltage [V]	37.3	39.1	38.5	39.7	40.9
	Issued Power [W]	26.89	46.44	96.64	116.58	119.63
	Calculated Power [W]	22.39	39.44	89.61	106.56	110.54
	Difference [W]	−4.50	−7.00	−7.03	−10.02	−9.09

Table 13. Maximum power differences between the calculated and the issued *I-V* characteristics of Kyocera KD245GH-4FB2, at irradiance $G = 1000 \text{ W/m}^2$.

Parameters at the Maximum Difference Points		Temperature [°C]		
		25	**50**	**75**
Hadj Arab *et al.* model	Voltage [V]	32.5	29.5	26.5
	Issued Power [W]	214.37	178.15	144.13
	Calculated Power [W]	218.90	189.42	161.18
	Difference [W]	4.53	11.27	17.05
De Soto *et al.* model	Voltage [V]	32.5	29.5	26.5
	Issued Power [W]	214.37	178.15	144.13
	Calculated Power [W]	219.88	187.68	156.31
	Difference [W]	5.51	9.53	12.18
Sera *et al.* model	Voltage [V]	34.5	31.0	27.5
	Issued Power [W]	148.52	132.62	116.63
	Calculated Power [W]	161.71	146.88	131.39
	Difference [W]	13.19	14.26	14.76
Villalva *et al.* model	Voltage [V]	34.0	31.0	27.5
	Issued Power [W]	169.73	132.62	116.63
	Calculated Power [W]	178.81	147.05	134.37
	Difference [W]	9.08	14.43	17.74
Lo Brano *et al.* model	Voltage [V]	36.2	29.0	26.0
	Issued Power [W]	54.30	188.94	154.70
	Calculated Power [W]	49.86	193.81	160.49
	Difference [W]	−4.44	4.87	5.79
Seddaoui *et al.* model	Voltage [V]	32.5	33.6	29.5
	Issued Power [W]	214.37	0.00	39.12
	Calculated Power [W]	218.90	26.35	83.75
	Difference [W]	4.53	26.35	44.63
Siddique *et al.* model	Voltage [V]	34.5	31.5	28.5
	Issued Power [W]	148.52	113.18	81.94
	Calculated Power [W]	165.12	139.35	114.35
	Difference [W]	16.60	26.17	32.41
Yetayew *et al.* model	Voltage [V]	32.5	33.6	30.2
	Issued Power [W]	54.30	0.00	4.98
	Calculated Power [W]	47.92	26.46	49.88
	Difference [W]	−6.38	26.46	44.90
Orioli *et al.* model	Voltage [V]	32.5	29.5	27.5
	Issued Power [W]	214.37	178.15	116.63
	Calculated Power [W]	221.53	185.86	125.47
	Difference [W]	7.16	7.71	8.84

Table 14. Maximum power differences between the calculated and the issued *I-V* characteristics of Sanyo HIT-240 HDE4, at irradiance G = 1000 W/m^2.

Parameters at the Maximum Difference Points		Temperature [°C]		
		25	**50**	**75**
Hadj Arab *et al.* model	Voltage [V]	42.7	39.7	37.3
	Issued Power [W]	45.73	57.22	41.80
	Calculated Power [W]	41.51	51.37	35.50
	Difference [W]	−4.22	−5.85	−6.30
De Soto *et al.* model	Voltage [V]	39.7	37.3	34.3
	Issued Power [W]	159.62	142.18	140.68
	Calculated Power [W]	184.86	159.12	151.09
	Difference [W]	25.24	16.94	10.41
Sera *et al.* model	Voltage [V]	40.6	38.2	35.5
	Issued Power [W]	131.28	113.78	105.97
	Calculated Power [W]	173.06	144.60	125.55
	Difference [W]	41.78	30.82	19.58
Villalva *et al.* model	Voltage [V]	39.7	38.2	34.3
	Issued Power [W]	159.62	113.78	140.68
	Calculated Power [W]	190.36	136.17	156.31
	Difference [W]	30.74	22.39	15.63
Lo Brano *et al.* model	Voltage [V]	42.7	40.6	37.9
	Issued Power [W]	45.73	18.46	16.62
	Calculated Power [W]	41.49	13.18	11.10
	Difference [W]	−4.24	−5.28	−5.52
Seddaoui *et al.* model	Voltage [V]	42.7	40.9	38.2
	Issued Power [W]	45.73	0.00	0.00
	Calculated Power [W]	41.51	15.68	31.74
	Difference [W]	−4.22	15.68	31.74
Siddique *et al.* model	Voltage [V]	40.6	38.2	35.5
	Issued Power [W]	131.28	113.78	105.97
	Calculated Power [W]	176.96	147.74	125.79
	Difference [W]	45.68	33.96	19.82
Yetayew *et al.* model	Voltage [V]	42.7	40.9	38.2
	Issued Power [W]	45.73	0.00	0.00
	Calculated Power [W]	40.73	16.21	32.76
	Difference [W]	−5.00	16.21	32.76
Orioli *et al.* model	Voltage [V]	40.9	39.7	34.9
	Issued Power [W]	119.63	57.22	125.32
	Calculated Power [W]	110.54	47.96	115.05
	Difference [W]	−9.09	−9.26	−10.27

For the Kyocera PV panel, the smallest MD(*P*)s at constant cell temperature are again obtained with the Lo Brano *et al.* model that yields values varying from −2.82 W to −8.83 W. The greatest

MD(*P*)s, which occur with the Siddique *et al.* and the Yetayew *et al.* models, are in the range −20.40 W to 21.32 W. For the Sanyo PV module, the smallest MD(*P*)s at constant temperature, which vary from −1.41 W to −6.19 W, are generated by the Hadj Arab *et al.*, the Lo Brano *et al.* and the Seddaoui *et al.* models. The De Soto *et al.*, the Siddique *et al.* and the Yetayew *et al.* models yield the greatest inaccuracies, which vary from 28.21 W to 45.68 W.

Considering the MD(*P*)s at constant solar irradiance, the smallest values for the Kyocera PV panel are obtained from the Lo Brano *et al.* model. The differences range from −4.44 W to 5.79 W. The greatest inaccuracies are provide by the Siddique *et al.* and the Yetayew *et al.* models. Differences, varying between 16.60 W and 44.90 W, were calculated. The Hadj Arab *et al.*, the Lo Brano *et al.*, and the Seddaoui *et al.* models yield the smallest MD(*P*)s for the Sanyo PV module, which are in the range from −4.22 W to −5.52 W. The greatest values are due to the Siddiqui *et al.* and the Yetayew *et al.* models. Such differences vary from 32.76 W to 45.68 W. In Tables 15 and 16, the percentage ratios of MAD(*I*) to the current at the issued MPP, and of MAD(*P*) to the rated maximum power, are listed. In the last column the average values of the ratios of MAD(*I*) to the current at the issued MPP, and of MAD(*P*) to the rated maximum power, calculated for all *I-V* curves, are listed.

Table 15. Percentage ratio of the mean absolute difference, MAD(*I*) to the rated current at the maximum power point.

PV Panel	*I-V* Characteristic	$MAD(I)/I_{mp,ref}$ [%]							
	Irradiance [W/m^2]	200	400	600	800	1000	1000	1000	Average Value
	Temperature [°C]	25	25	25	25	25	50	75	
Kyocera KD245GH-4FB2	Hadj Arab *et al.* model	1.34	1.86	1.58	1.35	0.51	1.52	2.43	1.51
	De Soto *et al.* model	1.23	1.81	1.60	1.51	0.63	1.41	1.65	1.41
	Sera *et al.* model	1.14	0.79	0.69	1.12	1.65	1.82	2.58	1.40
	Villalva *et al.* model	0.94	0.66	0.61	1.08	1.26	2.16	2.32	1.29
	Lo Brano *et al.* model	0.50	0.72	1.00	0.40	0.51	0.58	0.77	0.64
	Seddaoui *et al.* model	1.68	2.27	1.90	1.59	0.51	3.82	7.96	2.82
	Siddique *et al.* model	1.66	1.49	1.06	1.14	2.02	3.74	5.02	2.31
	Yetayew *et al.* model	2.54	3.07	2.33	1.65	0.62	3.49	7.91	3.09
	Orioli *et al.* model	0.92	1.30	1.40	0.51	0.78	1.07	1.37	1.05
Sanyo HIT-240 HDE4	Hadj Arab *et al.* model	3.40	4.79	4.77	2.75	0.31	0.52	0.97	2.50
	De Soto *et al.* model	2.56	4.22	4.92	4.53	3.57	3.03	2.23	3.58
	Sera *et al.* model	1.06	1.48	2.57	3.46	4.74	4.31	4.03	3.09
	Villalva *et al.* model	1.61	2.87	3.93	3.97	3.94	3.49	2.88	3.24
	Lo Brano *et al.* model	0.22	0.41	0.32	0.61	0.31	0.43	0.50	0.40
	Seddaoui *et al.* model	3.47	4.83	4.82	2.76	0.31	1.68	3.65	3.07
	Siddique *et al.* model	1.51	1.09	2.01	3.13	4.98	4.18	3.41	2.90
	Yetayew *et al.* model	3.71	5.11	5.02	2.81	0.35	1.58	3.72	3.19
	Orioli *et al.* model	0.83	1.17	1.11	1.48	1.15	1.51	1.73	1.28

Table 16. Percentage ratio of MAD(*P*) to the rated maximum power.

PV Panel	*I-V* Characteristic	MAD(*P*)/$V_{mp,ref}$ $I_{mp,ref}$ [%]							
	Irradiance [W/m^2]	200	400	600	800	1000	1000	1000	Average Value
	Temperature [°C]	25	25	25	25	25	50	75	
Kyocera KD245GH-4FB2	Hadj Arab *et al.* model	1.28	1.92	1.66	1.47	0.55	1.48	2.13	1.50
	De Soto *et al.* model	1.27	1.91	1.70	1.61	0.66	1.33	1.42	1.41
	Sera *et al.* model	1.16	0.85	0.72	1.17	1.74	1.75	1.98	1.34
	Villalva *et al.* model	0.94	0.72	0.66	1.14	1.30	2.02	2.02	1.26
	Lo Brano *et al.* model	0.51	0.76	1.10	0.44	0.55	0.54	0.66	0.65
	Seddaoui *et al.* model	1.76	2.44	2.04	1.72	0.55	3.85	7.43	2.83
	Siddique *et al.* model	1.70	1.59	1.10	1.17	2.13	3.59	4.61	2.27
	Yetayew *et al.* model	2.70	3.31	2.52	1.79	2.70	3.54	7.40	3.42
	Orioli *et al.* model	0.94	1.39	1.52	0.56	0.83	1.03	1.22	1.07
SanyoHIT-240 HDE4	Hadj Arab *et al.* model	3.60	5.17	5.21	3.01	0.34	0.54	0.94	2.69
	De Soto *et al.* model	2.65	4.47	5.24	4.74	3.61	2.80	1.87	3.63
	Sera *et al.* model	0.96	1.44	2.67	3.68	5.20	4.15	3.40	3.07
	Villalva *et al.* model	1.37	2.80	4.02	4.10	4.10	3.34	2.55	3.18
	Lo Brano *et al.* model	0.20	0.42	0.33	0.67	0.35	0.44	0.48	0.41
	Seddaoui *et al.* model	3.67	5.22	5.24	3.02	0.34	1.78	3.66	3.28
	Siddique *et al.* model	1.49	1.10	2.11	3.40	5.54	4.23	3.14	3.00
	Yetayew *et al.* model	3.92	5.53	5.46	3.06	0.40	1.68	3.74	3.40
	Orioli *et al.* model	0.82	1.21	1.17	1.58	1.23	1.51	1.64	1.31

For the Kyocera PV panel the smallest MAD(*I*)s range from 0.40% to 0.77% of the current at the MPP; the greatest MAD(*I*)s vary from 1.65% to 7.96%. The smallest MAD(*I*)s for the Sanyo PV module are in the range 0.22% to 0.61% of the current at the MPP; the greatest MAD(*I*)s range from 3.71% to 5.11%. The smallest MAD(*P*)s range from 0.44% to 0.72% of the rated maximum power for the Kyocera PV panel; the greatest MAD(*P*)s vary from 1.79% to 7.43%. For the Sanyo PV module the smallest MAD(*P*)s are in the range 0.20% to 0.67% of the rated maximum power; the greatest MAD(*P*)s vary from 3.74% to 5.54%.

5. Rating of the Usability and Accuracy of the One-Diode Models

As it was previously observed, the usability is a qualitative parameter whereas the accuracy level is quantitatively described. Even though it is not simple to find an index able to globally represent both the usability and accuracy of the considered analytical procedure, an attempt to get a concise description of the model performances, is necessary in order to define the rating criterion. The approach proposed, which is based on a three-level rating scale, takes into consideration the following features:

- the ease of finding the performance data used by the analytical procedure;
- the simplicity of the mathematical tools needed to perform calculations;
- the accuracy achieved in calculating the current and power of the analysed PV modules.

The ease of finding the input data is assumed:

- high, when only tabular data are required (short circuit current, open circuit voltage, MPP current and voltage;

- medium, when the data have to be extracted by reading the *I-V* characteristics (open circuit voltage at conditions different from the SRC, current and voltage of the 4th and 5th points);
- low, when the derivative of the *I-V* curves, at the short circuit and open circuit points, are required.

The simplicity of the used mathematical tools is considered:

- high, if only simple calculations are necessary;
- medium, if an iterative procedure is used;
- low, when the analytical procedure requires the use of dedicated computational software.

In order to condense the precision data, the results of the accuracy assessment are summarized in Table 17, where the average ratios of MAD(*I*) to the rated current at the MPP, and of MAD(*P*) to the rated maximum power, extracted from Table 15 and Table 16, are listed.

Table 17. Average ratios of MAD(*I*) to the rated current at the MPP andof MAD(*P*) to the rated maximum power.

MODEL	Average MAD(*I*)/$I_{mp,ref}$ [%]		Average MAD(*P*)/$V_{mp,ref} I_{mp,ref}$ [%]		Global Accuracy
	Kyocera KD245GH-4FB2	Sanyo HIT-240 HDE4	Kyocera KD245GH-4FB2	Sanyo HIT-240 HDE4	
Hadj Arab *et al.*	1.51	2.50	1.50	2.69	2.05
De Soto *et al.*	1.41	3.58	1.41	3.63	2.51
Sera *et al.*	1.40	3.09	1.34	3.07	2.23
Villalva *et al.*	1.29	3.24	1.26	3.18	2.24
Lo Brano *et al.*	0.64	0.40	0.65	0.41	0.53
Seddaoui *et al.*	2.82	3.07	2.83	3.28	3.00
Siddique *et al.*	2.31	2.90	2.27	3.00	2.62
Yetayew *et al.*	3.09	3.19	3.42	3.40	3.27
Orioli *et al.*	1.05	1.28	1.07	1.31	1.18

It can be observed that the global accuracy listed in Table 17, which is calculated averaging the accuracies evaluated for the Kyocera and Sanyo PV panels, ranges from 0.53% to 3.27%. Such range of variation was divided in three equal intervals, which were used to qualitatively describe the accuracy of the analysed models:

- high, for values of the mean difference in the subrange 0.52% to 1.39%;
- medium, for values of the mean difference in the subrange 1.39% to 2.26%;
- low, for values of the mean difference in the subrange 2.26% to 3.14%.

Table 18 lists the rating of the ease of finding data, simplicity of mathematical tools, and accuracy in calculating the current and power, based on the three-level rating scale previously described.

As it can be observed in Table 18, some models, such as De Soto *et al.*, Yetayew *et al.*, Villalva *et al.*, Siddique *et al.* have good level of usability, but reach a smaller accuracy. Adversely, some models, such as Hadj Arab *et al.*, Sera *et al.* and Lo Brano *et al.* are more accurate, but their usability is lower. Although the solving technique required by Seddaoui *et al.* model allows users to tackle a medium level of mathematical difficulty, the data finding results more elaborate and a low level of accuracy in the calculated current and power was obtained. As it was predictable, the choice of the one-diode model requires a wise compromise between usability and accuracy, which may prefer the usability to the accuracy, the accuracy to the usability, or try to find an acceptable balance between such features. No model achieved the highest rating for all the considered features. On the basis of the practical application of the proposed criterion, a medium degree of mathematical difficulty and a high level of current and power accuracy was provided by Orioli *et al.* model despite the major difficulty in the

data finding. The information, hypotheses and solving techniques required by the model represent the best possible compromise for researchers and designers to calculate precise and reliable parameters.

Table 18. Usability and accuracy rating of the analysed one-diode models.

MODEL	Ease of Data Finding	Mathematical Difficulty	Current and Power Accuracy
Hadj Arab *et al.*	Low	High	Medium
De Soto *et al.*	Medium	Low	Low
Sera *et al.*	Low	Medium	Medium
Villalva *et al.*	High	Medium	Medium
Lo Brano *et al.*	Low	Medium	High
Seddaoui *et al.*	Low	High	Low
Siddique *et al.*	High	Medium	Low
Yetayew *et al.*	Medium	Low	Low
Orioli *et al.*	High	Medium	High

6. Conclusions

A criterion for rating the usability and accuracy performances of diode-based equivalent circuits was tested on some one-diode models. In order to define the criterion an accurate examination of the used analytical procedures along with the comparison between calculated results and reference data was carried out. The procedures adopted by the tested models were minutely described and analysed along with the used performance data, simplifying hypotheses and mathematical methods needed to calculate the model parameters. Most of the performance data can be easily found, because they are always listed in the PV module datasheets, whereas some data can be extracted only if a complete set of *I-V* curves is provided by the manufacturers. Moreover, mathematical tools with different degrees of complexity, which include simple algorithms, iterative routines, mathematical methods or dedicated computer software, may be necessary to calculate the model parameters.

The tested models were implemented to calculate the *I-V* curves, at constant cell temperature and solar irradiance, of two different types of PV modules. The accuracy achievable with the one-diode models was assessed by comparing the calculated *I-V* curves with the *I-V* characteristics issued by manufactures and evaluating the maximum difference and the mean absolute difference between the calculated and issued values of current and power. Depending on the used model, the most effective one-diode equivalent circuits yielded for the poly-crystalline Kyocera KD245GH-4FB2 PV panel values of the current difference that averagely range from 0.40% to 0.77% of the current at the MPP. The values of the power difference averagely vary between 0.44% and 0.72% of the rated maximum power. For the Sanyo HIT-240 HDE4 PV module greater accuracies were generally observed. The current differences averagely vary from 0.22% to 0.61% of the current at the MPP. The power accuracies averagely range from 0.20% to 0.67% of the rated maximum power. The accuracies of the less effective models averagely reach 7.96% of the current at the MPP and 7.43% of the rated maximum power for the Kyocera PV panel, whereas average differences of 5.11% of the current at the MPP and of 5.54% of the rated maximum power were observed for the Sanyo PV module.

In order to rate both the usability and accuracy of the considered analytical procedure, a three-level rating scale (high, medium and low) was defined considering some significant features, such as the ease of finding the performance data used by the analytical procedure, the simplicity of the mathematical tools needed to perform calculations and the accuracy achieved in calculating the current and power of the analysed PV modules. No model achieved the highest rating for all the considered features. As it was predictable, the selection of the one-diode model requires that researchers and PV designers, who are the only persons aware of the peculiarities of the problem to be solved, reach a suitable compromise between analytical complexity and expected accuracy. In our opinion, even though the presented criterion is obviously debatable and other approaches may be used to rate the usability and accuracy of the one-diode models, the information provided in this paper may be useful to make more aware choices and support the users in implementing the selected model.

Nomenclature

a	diode shape factor
G	solar irradiance (W/m^2)
G_{ref}	solar irradiance at the SRC (1000 W/m^2)
I	current generated by the panel (A)
$I_{calc,j}$	current of the *j*-th calculated point of the *I-V* characteristic (A)
$I_{iss,j}$	current of the *j*-th point extracted from the issued *I-V* characteristic (A)
I_L	photocurrent (A)
$I_{L,ref}$	photocurrent (A) at the SRC (A)
$I_{mp,ref}$	current in the maximum power point at the SRC (A)
I_{sc}	short circuit current of the panel (A)
$I_{sc,ref}$	short circuit current of the panel at the SRC (A)
I_0	diode saturation current (A)
$I_{0,ref}$	diode saturation current at the SRC (A)
$I_{L,ref}$	photocurrent (A) at the SRC (A)
$I_{mp,ref}$	current in the maximum power point at the SRC (A)
I_{sc}	short circuit current of the panel (A)
$I_{sc,ref}$	short circuit current of the panel at the SRC (A)
I_0	diode saturation current (A)
$I_{0,ref}$	diode saturation current at the SRC (A)
k	Boltzmann constant (J/K)
K	thermal correction factor ($\Omega/^\circ$C)
n	diode quality factor (V/K)
N	number of points extracted from the issued *I-V* characteristic
N_{cs}	number of cells connected in series
P	power generated by the panel (W)
q	electron charge (C)
R_s	series resistance (Ω)
R_{so}	reciprocal of slope of the *I-V* characteristic for $V = V_{oc}$ and $I = 0$ (Ω)
$R_{s,ref}$	series resistance at the SRC (Ω)
R_{sh}	shunt resistance (Ω)
R_{sho}	reciprocal of slope of the *I-V* characteristic for $V = 0$ and $I = I_{sc}$ (Ω)
$R_{sh,ref}$	shunt resistance at the SRC (Ω)
T	temperature of the PV cell ($^\circ$K)
T_{ref}	temperature of the PV panel at the SRC (25 $^\circ$C – 298.15°K)
V	voltage generated by the PV panel (V)
V_{oc}	open circuit voltage of the PV panel (V)
$V_{oc,ref}$	open circuit voltage of the PV panel at the SRC (V)
$V_{iss,j}$	voltage of the *j*-th point extracted from the issued *I-V* characteristic (A)
$V_{mp,ref}$	voltage in the maximum power point at the SRC (V)
α_G	ratio of the current irradiance to the irradiance at SRC
γ	diode ideality factor
ε_G	bandgap energy of the material (eV)
$\mu_{I,sc}$	thermal coefficient of the short circuit current (A/$^\circ$C)
$\mu_{V,oc}$	thermal coefficient of the open circuit voltage (V/$^\circ$C)

Appendix

In this appendix the equations used by the various one-diode models to describe the physical properties of PV panels are reviewed along with the analytical procedures adopted to get the explicit or implicit expressions necessary to calculate the equivalent model parameters.

A1. Kennerud Model

To make the calculated curve coincide with an experimental curve, the following information is considered:

(1) short circuit point ($I = I_{sc,ref}$; $V = 0$);
(2) open circuit point ($I = 0$; $V = V_{oc,ref}$);
(3) derivative of current at the short circuit point ($\partial(I)/\partial V = -1/R_{sho}$ at $I = I_{sc,ref}$; $V = 0$);
(4) derivative of current at the open circuit point ($\partial(I)/\partial V = -1/R_{so}$ at $I = 0$; $V = V_{oc,ref}$);
(5) derivative of power at the MPP ($\partial P/\partial V = 0$ at $I = I_{mp,ref}$; $V = V_{mp,ref}$).

The fifth piece of information, which is described by the following relation:

$$\left.\frac{\partial P}{\partial V}\right|_{\substack{V = V_{mp,ref} \\ I = I_{mp,ref}}} = \left.\frac{\partial(VI)}{\partial V}\right|_{\substack{V = V_{mp,ref} \\ I = I_{mp,ref}}} = I_{mp,ref} + V_{mp,ref}\left.\frac{\partial I}{\partial V}\right|_{\substack{V = V_{mp,ref} \\ I = I_{mp,ref}}} = 0 \tag{A1}$$

can also be written as:

$$\left.\frac{\partial I}{\partial V}\right|_{\substack{V = V_{mp,ref} \\ I = I_{mp,ref}}} = -\frac{I_{mp,ref}}{V_{mp,ref}} \tag{A2}$$

The derivative of Equation (2) with respect to the voltage is:

$$\frac{\partial I}{\partial V} = -\frac{I_0}{nT}\left(1 + R_s\frac{\partial I}{\partial V}\right)e^{\frac{V+IR_s}{nT}} - \frac{1}{R_{sh}}\left(1 + R_s\frac{\partial I}{\partial V}\right) \tag{A3}$$

Using Equations (A2) and (A3), the five pieces of information are described by the following equations:

(1) $I = I_{sc,ref}$; $V = 0$:

$$I_{sc,ref} = I_{L,ref} - I_{0,ref}\left(e^{\frac{I_{sc,ref}R_s}{nT_{ref}}} - 1\right) - \frac{I_{sc,ref}R_s}{R_{sh}} \tag{A4}$$

(2) $I = 0$; $V = V_{oc,ref}$:

$$0 = I_{L,ref} - I_{0,ref}\left(e^{\frac{V_{oc,ref}}{nT_{ref}}} - 1\right) - \frac{V_{oc,ref}}{R_{sh}} \tag{A5}$$

(3) $\partial I/\partial V = -1/R_{sho}$ at $I = I_{sc,ref}$; $V = 0$:

$$\frac{I_{0,ref}}{nT_{ref}}\left(1 - \frac{R_s}{R_{sho}}\right)e^{\frac{I_{sc,ref}R_s}{nT_{ref}}} + \frac{1}{R_{sh}}\left(1 - \frac{R_s}{R_{sho}}\right) = \frac{1}{R_{sho}} \tag{A6}$$

(4) $\partial I/\partial V = -1/R_{so}$ at $I = 0$; $V = V_{oc,ref}$:

$$\frac{I_{0,ref}}{nT_{ref}}\left(1 - \frac{R_s}{R_{so}}\right)e^{\frac{V_{oc,ref}}{nT_{ref}}} + \frac{1}{R_{sh}}\left(1 - \frac{R_s}{R_{so}}\right) = \frac{1}{R_{so}} \tag{A7}$$

(5) $\partial P / \partial V = 0$ at $I = I_{mp,ref}$; $V = V_{mp,ref}$:

$$\frac{I_{0,ref}}{nT_{ref}} \left(1 - R_s \frac{I_{mp,ref}}{V_{mp,ref}} \right) e^{\frac{V_{mp,ref} + I_{mp,ref} R_s}{nT_{ref}}} + \frac{1}{R_{sh}} \left(1 - R_s \frac{I_{mp,ref}}{V_{mp,ref}} \right) = \frac{I_{mp,ref}}{V_{mp,ref}} \tag{A8}$$

Using the above five pieces of information, Equations (A4)–(A8), listed in the appendix, are written and solved using the Newton-Raphson technique in order to calculate the model parameters $I_{L,ref}$, $I_{0,ref}$, R_s, R_{sh} and n. The model cannot be used for any value of solar irradiance and cell temperature because Kennerud described the operation of PV devices at only the SRC.

A2. Phang et al. Model

Phang *et al.* calculate the model parameters by means of the following information:

(1)   short circuit point ($I = I_{sc,ref}$; $V = 0$);
(2)   open circuit point ($I = 0$; $V = V_{oc,ref}$);
(3)   derivative of current at the short circuit point ($\partial I / \partial V = -1 / R_{sho}$ at $I = I_{sc,ref}$; $V = 0$);
(4)   derivative of current at the open circuit point ($\partial I / \partial V = -1 / R_{so}$ at $I = 0$; $V = V_{oc,ref}$);
(5)   MPP ($I = I_{mp,ref}$; $V = V_{mp,ref}$).

The first four pieces of information are described by Equations (A4)–(A7); the fifth piece of information corresponds to the equation:

$$I_{mp,ref} = I_{L,ref} - I_{0,ref} \left(e^{\frac{V_{mp,ref} + I_{mp,ref} R_s}{nT_{ref}}} - 1 \right) - \frac{V_{mp,ref} + I_{mp,ref} R_s}{R_{sh}} \tag{A9}$$

The following expressions of $I_{L,ref}$ are obtained from Equations (A4) and (A5):

$$I_{L,ref} = I_{sc,ref} + I_{0,ref} \left(e^{\frac{I_{sc,ref} R_s}{nT_{ref}}} - 1 \right) + \frac{I_{sc,ref} R_s}{R_{sh}} \tag{A10}$$

$$I_{L,ref} = I_{0,ref} \left(e^{\frac{V_{oc,ref}}{nT_{ref}}} - 1 \right) + \frac{V_{oc,ref}}{R_{sh}} \tag{A11}$$

in order to be substituted in Equations (A5) and (A9), respectively. After some manipulations. Equations (A5)–(A7) and (A10) can be rewritten in the following forms:

$$I_{0,ref} \left(e^{\frac{V_{oc,ref}}{nT_{ref}}} - e^{\frac{I_{sc,ref} R_s}{nT_{ref}}} \right) - I_{sc,ref} \left(1 + \frac{R_s}{R_{sh}} \right) + \frac{V_{oc,ref}}{R_{sh}} = 0 \tag{A12}$$

$$\frac{1}{R_{sh}} - \frac{1}{R_{sho} - R_s} + \frac{I_{0,ref}}{nT_{ref}} e^{\frac{I_{sc,ref} R_s}{nT_{ref}}} = 0 \tag{A13}$$

$$(R_{so} - R_s) \left(\frac{1}{R_{sh}} + \frac{I_{0,ref}}{nT_{ref}} e^{\frac{V_{oc,ref}}{nT_{ref}}} \right) - 1 = 0 \tag{A14}$$

$$I_{0,ref} e^{\frac{V_{oc,ref}}{nT_{ref}}} + \frac{V_{oc,ref} - V_{mp,ref}}{R_{sh}} - I_{mp,ref} \left(1 + \frac{R_s}{R_{sh}} \right) - I_{0,ref} e^{\frac{V_{mp,ref} + I_{mp,ref} R_s}{nT_{ref}}} = 0 \tag{A15}$$

Assuming the following hypotheses:

$$e^{\frac{V_{oc,ref}}{nT_{ref}}} >> e^{\frac{I_{sc,ref} R_s}{nT_{ref}}} \quad \frac{I_{0,ref}}{nT_{ref}} e^{\frac{V_{oc,ref}}{nT_{ref}}} >> \frac{1}{R_{sh}} \quad R_s << R_{sh} \quad \frac{I_{0,ref}}{nT_{ref}} e^{\frac{I_{sc,ref} R_s}{nT_{ref}}} << \frac{1}{R_{sh}} - \frac{1}{R_{sho} - R_s} \tag{A16}$$

Equations (A12)–(A15) are significantly simplified and, after some manipulations, the model parameters can be calculated by means of the following explicit forms:

$$R_{sh} = R_{sho} \tag{A17}$$

$$n = \frac{V_{mp,ref} + I_{mp,ref} R_{so} - V_{oc,ref}}{T_{ref} \left[\ln \left(I_{sc,ref} - \frac{V_{mp,ref}}{R_{sho}} - I_{mp,ref} \right) - \ln \left(I_{sc,ref} - \frac{V_{oc,ref}}{R_{sho}} \right) + \frac{I_{mp,ref}}{I_{sc,ref} - V_{oc,ref}/R_{sho}} \right]} \tag{A18}$$

$$I_{0,ref} = \left(I_{sc,ref} - \frac{V_{oc,ref}}{R_{sho}} \right) e^{-\frac{V_{oc,ref}}{nT_{ref}}} \tag{A19}$$

$$R_s = R_{so} - \frac{nT_{ref}}{I_{0,ref}} e^{-\frac{V_{oc,ref}}{nT_{ref}}} \tag{A20}$$

$$I_{L,ref} = I_{0,ref} \left(e^{\frac{I_{sc,ref} R_s}{nT_{ref}}} - 1 \right) + I_{sc,ref} \left(1 + \frac{R_s}{R_{sho}} \right) \tag{A21}$$

The model parameters are calculated by means of explicit Equations (A17)–(A21). Phang *et al.* only calculate the *I-V* characteristic at the SRC.

A3. de Blas et al. Model

The same five pieces of information adopted by Phang *et al.* are used by de Blas *et al.* and the following hypotheses are assumed:

$$e^{\frac{V_{oc,ref}}{nT_{ref}}} >> e^{\frac{I_{sc,ref} R_s}{nT_{ref}}} \qquad \frac{I_{0,ref}}{nT_{ref}} e^{\frac{V_{oc,ref}}{nT_{ref}}} << \frac{1}{R_{sh}} \tag{A22}$$

If Equation (A11) is substituted in Equation (A4), and the first of the hypotheses in Equation (A22) is considered, the diode reverse saturation current can be calculated as:

$$I_{0,ref} = \frac{I_{sc,ref} \left(1 + \frac{R_s}{R_{sh}} \right) - \frac{V_{oc,ref}}{R_{sho}}}{e^{\frac{V_{oc,ref}}{nT_{ref}}}} \tag{A23}$$

Moreover, if Equations (A11) and (A23) are used in Equation (A9), it is possible to write parameter *n* in the following form:

$$n = \frac{V_{mp,ref} + I_{mp,ref} R_s - V_{oc,ref}}{T_{ref} \ln \left[\frac{(I_{sc,ref} - I_{mp,ref})(1 + R_s/R_{sh}) - V_{mp,ref}/R_{sh}}{I_{sc,ref}(1 + R_s/R_{sh}) - V_{mp,ref}/R_{sh}} \right]} \tag{A24}$$

From Equation (A3) it is possible to extract the general form of the derivative of the current:

$$\frac{\partial I}{\partial V} = - \frac{\frac{I_0}{nT} e^{\frac{V + IR_s}{nT}} + \frac{1}{R_{sh}}}{1 + R_s \left(\frac{I_0}{nT} e^{\frac{V + IR_s}{nT}} + \frac{1}{R_{sh}} \right)} \tag{A25}$$

and use it to write the conditions regarding the derivatives in the short circuit and open circuit points at the SRC:

$$\left. \frac{\partial I}{\partial V} \right|_{\substack{V = 0 \\ I = I_{sc,ref}}} = - \frac{\frac{I_{0,ref}}{nT_{ref}} e^{\frac{I_{sc,ref} R_s}{nT_{ref}}} + \frac{1}{R_{sh}}}{1 + R_s \left(\frac{I_{0,ref}}{nT_{ref}} e^{\frac{I_{sc,ref} R_s}{nT_{ref}}} + \frac{1}{R_{sh}} \right)} = - \frac{1}{R_{sho}} \tag{A26}$$

$$\left.\frac{\partial I}{\partial V}\right|_{\substack{V = V_{oc,ref} \\ I = 0}} = -\frac{\frac{I_{0,ref}}{nT_{ref}}e^{\frac{V_{oc,ref}}{nT_{ref}}} + \frac{1}{R_{sh}}}{1 + R_s \left(\frac{I_{0,ref}}{nT_{ref}}e^{\frac{V_{oc,ref}}{nT_{ref}}} + \frac{1}{R_{sh}}\right)} = -\frac{1}{R_{so}} \tag{A27}$$

Due to the second hypothesis in Equation (A22), it is possible to extract the following expression from Equation (A26):

$$R_{sh} = R_{sho} - R_s \tag{A28}$$

If Equation (A23) is substituted in Equation (A26), resistance R_s can be calculated with the following equation:

$$R_s = \frac{R_{so}\left(\frac{V_{oc,ref}}{nT_{ref}} - 1\right) + R_{sho}\left(1 - \frac{I_{sc,ref}R_{so}}{nT_{ref}}\right)}{\frac{V_{oc,ref} - I_{sc,ref}R_{sho}}{nT_{ref}}} \tag{A29}$$

The resolution of the equations requires an iterative procedure based on the following steps:

(1)   an initial value of R_s is assumed;
(2) R_{sh} is calculated by Equation (A28);
(3) n is calculated by Equation (A24);
(4) $I_{0,ref}$ is calculated by Equation (A23);
(5) $I_{L,ref}$ is calculated by Equation (A11);
(6) R_s is calculated by Equation (A29);
(7)   the initial value of R_s is compared with the value calculated by Equation (A29);
(8)   the analytical procedure is concluded if the comparison is satisfied within a fixed accuracy; otherwise, a new value of R_s is assumed and the iterative procedure is repeated.

In order to use the model in conditions different from the SRC, de Blas *et al.* adopt for the diode reverse saturation current the equation proposed by Townsend [88]:

$$I_0(T) = I_{0,ref}\left(\frac{T}{T_{ref}}\right)^3 e^{\frac{q\varepsilon_G}{ak}\left(\frac{1}{T_{ref}} - \frac{1}{T}\right)} \tag{A30}$$

in which ε_G is the bandgap energy of the material. Moreover, de Blas *et al.* suggest calculating the model parameters by means of the values of the short circuit current and open circuit voltage measured under the specific cell temperature and solar irradiance conditions. Unfortunately, the measured values of the short circuit current and open circuit voltage are often unavailable and the values that may be extracted from the *I-V* curves issued by the manufacturer only refer to some particular values of solar irradiance and/or cell temperature.

A4. Hadj Arab, Chenlo and Benghanem Model

The Hadj Arab *et al.* model is an improvement of the Phang *et al.* model that permits to evaluate the *I-V* characteristics for values of solar irradiance and silicon temperature different from the SRC. Because the model parameters obtained with Equations (A17)–(A21) are only valid for the values of irradiance and temperature in correspondence of which they were calculated, Hadj Arab *et al.* use the method of Chenlo *et al.* [89] that permits to translate the *I-V* curve, referred to irradiance G_1 and temperature T_1, to other irradiance G_2 and temperature T_2. Any point (I_1, V_1) of the *I-V* characteristic is shifted to a new point (I_2, V_2) and the curve is translated without distorting its shape. The procedure is based on the following equations:

$$I_2 = I_1 + I_{sc}(G_2, T_2) - I_{sc}(G_1, T_1) \tag{A31}$$

$$V_2 = V_1 + V_{oc}(G_2, T_2) - V_{oc}(G_1, T_1) \tag{A32}$$

$$I_{sc}(G_2, T_2) = I_{sc}(G_1, T_1)\frac{G_2}{G_1} + \mu_{I,sc}(T_2 - T_1) \tag{A33}$$

$$V_{oc}(G_2, T_2) = V_{oc}(G_1, T_1) + nT_1\ln\left(\frac{G_2}{G_1}\right) + \mu_{V,oc}(T_2 - T_1) \tag{A34}$$

where $\mu_{I,sc}$ and $\mu_{V,oc}$ are the short circuit current and the open circuit voltage thermal coefficients, respectively.

A5. De Soto, Klein and Beckman Model

The first four pieces of information correspond to Equations (A4), (A5), (A9) and (A8), respectively. The last piece of information permits to write the following equation:

$$0 = I_L(G_{ref}, T) - I_0(T)\left(e^{\frac{V_{oc}(T)}{nT}} - 1\right) - \frac{V_{oc}(T)}{R_{sh}} \tag{A35}$$

that requires the use of appropriate relations for $I_L(G_{ref}, T)$, $I_0(T)$ and $V_{oc}(T)$. Equation (A35) is calculated assuming the following relations for the photocurrent, the open circuit voltage and the shunt resistance:

$$I_L(G, T) = I_{L,ref}\frac{G}{G_{ref}} + \mu_{I,sc}\left(T - T_{ref}\right) \tag{A36}$$

$$V_{oc}(T) = V_{oc,ref} + \mu_{V,oc}\left(T - T_{ref}\right) \tag{A37}$$

$$R_{sh}(G) = R_{sh,ref}\frac{G_{ref}}{G} \tag{A38}$$

in which $R_{sh,ref}$ is the value of the shunt resistance evaluated at SRC. Diode saturation current $I_0(T)$ is calculated with Equation (A35) in which the silicon bandgap energy is described by the following form:

$$\varepsilon_G = 1.121\left[1 - 0.0002677\left(T - T_{ref}\right)\right] \tag{A39}$$

The simultaneous solution of Equations (A4), (A5), (A9), (A8) and (A35), which is necessary to calculate the model parameters, is facilitated by a non-linear equation solver, such as EES [88].

A6. Sera, Teodorescu and Rodriguez Model

Assuming the following hypotheses:

$$e^{\frac{V_{oc,ref}}{nT_{ref}}} \gg 1 \qquad e^{\frac{I_{sc,ref}R_s}{nT_{ref}}} \gg 1 \qquad e^{\frac{V_{mp,ref}+I_{mp,ref}R_s}{nT_{ref}}} \gg 1 \qquad e^{\frac{V_{oc,ref}}{nT_{ref}}} \gg e^{\frac{I_{sc,ref}R_s}{nT_{ref}}} \qquad R_{sh} = R_{sho} \tag{A40}$$

Equations (A4), (A5) and (A9), which refer to the first three pieces of information, are rewritten as:

$$I_{sc,ref} = I_{L,ref} - I_{0,ref}e^{\frac{I_{sc,ref}R_s}{nT_{ref}}} - \frac{I_{sc,ref}R_s}{R_{sh}} \tag{A41}$$

$$0 = I_{L,ref} - I_{0,ref}e^{\frac{V_{oc,ref}}{nT_{ref}}} - \frac{V_{oc,ref}}{R_{sh}} \tag{A42}$$

$$I_{mp,ref} = I_{L,ref} - I_{0,ref}e^{\frac{V_{mp,ref}+I_{mp,ref}R_s}{nT_{ref}}} - \frac{V_{mp,ref} + I_{mp,ref}R_s}{R_{sh}} \tag{A43}$$

Photocurrent $I_{L,ref}$ can be extracted from Equation (A42):

$$I_{L,ref} = I_{0,ref}e^{\frac{V_{oc,ref}}{nT_{ref}}} + \frac{V_{oc,ref}}{R_{sh}} \tag{A44}$$

and substituted in Equation (A41) in order to write the following expression:

$$I_{0,ref} = \left(I_{sc,ref} - \frac{V_{oc,ref} - I_{sc,ref}R_s}{R_{sh}}\right) e^{-\frac{V_{oc,ref}}{nT_{ref}}} \tag{A45}$$

If Equation (A45) is used in Equation (A43):

$$I_{mp,ref} = I_{sc,ref} - \frac{V_{mp,ref} + \left(I_{mp,ref} - I_{sc,ref}\right)R_s}{R_{sh}} - \left(I_{sc,ref} - \frac{V_{oc,ref} - I_{sc,ref}R_s}{R_{sh}}\right) e^{\frac{V_{mp,ref} + I_{mp,ref}R_s - V_{oc,ref}}{nT_{ref}}} \tag{A46}$$

parameter n can be calculated with the following form:

$$n = \frac{V_{mp,ref} + I_{mp,ref}R_s - V_{oc,ref}}{T_{ref}\ln\left[\frac{\left(I_{sc,ref} - I_{mp,ref}\right)\left(R_s + R_{sh}\right) - V_{mp,ref}}{I_{sc,ref}\left(R_s + R_{sh}\right) - V_{oc,ref}}\right]} \tag{A47}$$

The fourth piece of information is described by Equation (A1) that, using Equations (A25) and (A42), becomes:

$$\left.\frac{\partial P}{\partial V}\right|_{\substack{V = V_{mp,ref} \\ I = I_{mp,ref}}} = I_{mp,ref} - \frac{V_{mp,ref}\left[\frac{I_{sc,ref}\left(R_{sh} + R_s\right) - V_{oc,ref}}{nTR_{sh}}e^{\frac{V_{mp,ref} + I_{mp,ref}R_s - V_{oc,ref}}{nT_{ref}}} + \frac{1}{R_{sh}}\right]}{1 + R_s\left(\frac{I_{sc,ref}\left(R_{sh} + R_s\right) - V_{oc,ref}}{nTR_{sh}}e^{\frac{V_{mp,ref} + I_{mp,ref}R_s - V_{oc,ref}}{nT_{ref}}} + \frac{1}{R_{sh}}\right)} = 0 \tag{A48}$$

Due to the last hypothesis in Equation (A40), the condition about the derivative of current at the short circuit point is described by the following equation:

$$\left.\frac{\partial I}{\partial V}\right|_{\substack{V = 0 \\ I = I_{sc,ref}}} = -\frac{\frac{I_{sc,ref}\left(R_{sh} + R_s\right) - V_{oc,ref}}{nTR_{sh}}e^{\frac{I_{sc,ref}R_s - V_{oc,ref}}{nT_{ref}}} + \frac{1}{R_{sh}}}{1 + R_s\left(\frac{I_{sc,ref}\left(R_{sh} + R_s\right) - V_{oc,ref}}{nTR_{sh}}e^{\frac{I_{sc,ref}R_s - V_{oc,ref}}{nT_{ref}}} + \frac{1}{R_{sh}}\right)} = -\frac{1}{R_{sh}} \tag{A49}$$

The model parameters can be calculated with Equations (A44), (A45), (A47), (A48) and (A49). Due to the presence of implicit forms, the iterative procedure based on the following steps has to be used:

(1) an initial values of R_s is assumed;
(2) an initial values of R_{sh} is assumed;
(3) n is calculated by Equation (A47);
(4) Equation (A48) is calculated;
(5) the value of R_{sh} is modified and steps 3 and 4 are repeated until Eq. (A48) is verified within a fixed accuracy;
(6) Equation (A49) is calculated;
(7) the iterative procedure is concluded if Equation (A49) is verified within a fixed accuracy; otherwise, a new value of R_s is assumed and steps 2, 3, 4, 5 and 6 are repeated.
(8) $I_{0,ref}$ is calculated by Equation (A45);

(9)　$I_{L,ref}$ is calculated by Equation (A44).

In order to describe the electrical behaviour of the analysed PV device far from the SRC, the values of I_0 and I_L in Equation (2) are updated using the following equations:

$$I_0 = \left(I_{sc} - \frac{V_{oc} + I_{sc}R_s}{R_{sh}} \right) e^{-\frac{V_{oc}}{nT}} \tag{A50}$$

$$I_L = I_0 e^{\frac{V_{oc}}{nT}} + \frac{V_{oc}}{R_{sh}} \tag{A51}$$

in which the dependence of I_{sc} and V_{oc} on the solar irradiance and cell temperature is calculated with the following relations:

$$I_{sc}(G,T) = I_{sc,ref}\frac{G}{G_{ref}} + \mu_{I,sc}\left(T - T_{ref} \right) \tag{A52}$$

$$V_{oc}(G,T) = V_{oc}(G) + \mu_{V,oc}\left(T - T_{ref} \right) \tag{A53}$$

To calculate $V_{oc}(G)$, the following equation, which is derived from Equation (A42), has to be numerically solved:

$$V_{oc}(G) = nT_{ref}\ln\left[\frac{I_L(G)R_{sh} - V_{oc}(G)}{I_{0,ref}R_{sh}} \right] \tag{A54}$$

in which the following expression is assumed for $I_L(G)$:

$$I_L(G) = I_{L,ref}\frac{G}{G_{ref}} \tag{A55}$$

A7. Villalva, Gazoli and Filho Model

If the following hypotheses are assumed:

$$e^{\frac{I_{sc,ref}R_s}{nT_{ref}}} \approx 1 \qquad \frac{V_{oc,ref}}{R_{sh}} \approx 0 \tag{A56}$$

the short circuit and open circuit conditions permit to write the following expressions:

$$I_{L,ref} = \frac{R_{sh} + R_s}{R_{sh}}I_{sc,ref} \tag{A57}$$

$$I_{0,ref} = \frac{I_{L,ref}}{e^{\frac{V_{oc,ref}}{nT_{ref}}} - 1} \tag{A58}$$

The third and fourth pieces of information correspond to the following equations:

$$I_{mp,ref} = I_{L,ref} - I_{0,ref}\left(e^{\frac{V_{mp,ref} + I_{mp,ref}R_s}{nT_{ref}}} - 1 \right) - \frac{V_{mp,ref} + I_{mp,ref}R_s}{R_{sh}} \tag{A59}$$

$$P_{mp,ref} = V_{mp,ref}I_{mp,ref} = V_{mp,ref}\left[I_{L,ref} - I_{0,ref}\left(e^{\frac{V_{mp,ref} + I_{mp,ref}R_s}{nT_{ref}}} - 1 \right) - \frac{V_{mp,ref} + I_{mp,ref}R_s}{R_{sh}} \right] \tag{A60}$$

where $P_{mp,ref}$ is value of the experimental peak power issued on datasheets or measured. Shunt resistance R_{sh} can be extracted from Equation (A60):

$$R_{sh} = \frac{V_{mp,ref}\left(V_{mp,ref} + I_{mp,ref}R_s\right)}{V_{mp,ref}\left[I_{L,ref} - I_{0,ref}\left(e^{\frac{V_{mp,ref}+I_{mp,ref}R_s}{nT_{ref}}} - 1\right)\right] - P_{mp,ref}} \tag{A61}$$

the first four pieces of information correspond to Equations (A57)–(A60) listed in the appendix. Such equations are modified to consider the effect of the solar irradiance and cell temperature by means of the following relations:

$$I_L = \left[I_{L,ref} + \mu_{I,sc}\left(T - T_{ref}\right)\right]\frac{G}{G_{ref}} \tag{A62}$$

$$I_0 = \frac{I_{sc,ref} + \mu_{I,sc}\left(T - T_{ref}\right)}{e^{\frac{V_{oc,ref}+\mu_{V,oc}(T-T_{ref})}{nT_{ref}}} - 1} \tag{A63}$$

In order to calculate the model parameters, an iterative procedure is used. The goal is to find the value of R_s, and hence of R_{sh} from Equation (A61), that makes the peak of the mathematical power-voltage curve coincide with $P_{mp,ref}$. The following iterative method is adopted:

(1) a fixed value of *a* is used to calculate $n = aN_{cs}k/q$;
(2) an initial values of R_{sh} is assumed;
(3) an initial values of R_s is assumed;
(4) I_L is calculated by Equation (A57);
(5) I_0 is calculated by Equation (A58);
(6) R_{sh} is calculated by Equation (A61);
(7) Equation (2) is used in order to find the MPP and calculate the maximum power;
(8) the calculated maximum power is compared with the issued value of $P_{mp,ref}$;

the iterative procedure is concluded if the comparison is satisfied within a fixed accuracy; otherwise, a new value of R_s is assumed and steps 4, 5, 6 ,7 and 8 are repeated.

Villalva *et al.* use a value of *a* = 1.3 and the following initial values of the series and shunt resistances:

$$R_s = 0 \qquad R_{sh} = \frac{V_{mp,ref}}{I_{sc,ref} - I_{mp,ref}} - \frac{V_{oc,ref} - V_{mp,ref}}{I_{mp,ref}} \tag{A64}$$

A8. Lo Brano, Orioli, Ciulla and Di Gangi Model

The used information permits to write Equations (A4), (A5), (A9), (A26) and (A27) from which the following expressions can be extracted:

$$I_{L,ref} = \left(1 + \frac{R_{s,ref}}{R_{sh,ref}}\right)I_{sc,ref} + I_{0,ref}\left(e^{\frac{I_{sc,ref}R_{s,ref}}{nT_{ref}}} - 1\right) \tag{A65}$$

$$n = \frac{V_{oc,ref}}{T\ln\left[1 + \frac{I_{L,ref}-V_{oc,ref}/R_{sh,ref}}{I_{0,ref}}\right]} \tag{A66}$$

$$I_{0,ref} = \frac{I_{L,ref} - I_{mp,ref} - \frac{V_{mp,ref}+I_{mp,ref}R_{s,ref}}{R_{sh,ref}}}{e^{\frac{V_{mp,ref}+I_{mp,ref}R_{s,ref}}{nT_{ref}}} - 1} \tag{A67}$$

$$R_{sh,ref} = \frac{R_{sho} - R_{s,ref}}{1 - \left(R_{sho} - R_{s,ref}\right)\frac{I_{0,ref}}{nT_{ref}}e^{\frac{I_{sc,ref}R_{s,ref}}{nT_{ref}}}} \tag{A68}$$

$$R_{s,ref} = \frac{R_{so}\left(\frac{I_{0,ref}}{nT_{ref}}e^{\frac{V_{oc,ref}}{nT_{ref}}} + \frac{1}{R_{sh,ref}}\right) - 1}{\frac{I_{0,ref}}{nT_{ref}}e^{\frac{V_{oc,ref}}{nT_{ref}}} + \frac{1}{R_{sh,ref}}} \tag{A69}$$

The model parameters are calculated using the implicit Equations (A65)–(A68) and (A69), which are solved with a numerical procedure based on a double process of trial and error for the parameters R_s and n with the second process nested into the first. To start the process, it is necessary to use the following positions:

$$I_{L,ref} = I_{sc,ref} \qquad R_{sh,ref} = R_{sho} \tag{A70}$$

To calculate the model parameters, the following sequence of steps is adopted:

(1) the initial values of $I_{L,ref}$ and $R_{sh,ref}$ from Equation (A70) are set;
(2) an initial values of $R_{s,ref}$ is assumed;
(3) an initial values of n is assumed;
(4) $I_{0,ref}$ is calculated by Equation (A67);
(5) $I_{L,ref}$ is calculated by Equation (A65);
(6) $R_{sh,ref}$ is calculated by Equation (A68);
(7) the current value of n is compared with the value calculated with Equation (A66);
(8) the current value of n is modified and steps 4, 5, 6 and 7 are repeated until Equation (A66) is verified within a fixed accuracy;
(9) the current value of $R_{s,ref}$ is compared with the value calculated with Equation (A69);
(10) the iterative procedure is concluded if Equation (A69) is verified within a fixed accuracy; otherwise, a new value of $R_{s,ref}$ is assumed and steps 3, 4, 5, 6, 7, 8 and 9 are repeated.

To increase the robustness of the iterative procedure, the input data $V_{oc,ref}$, $I_{sc,ref}$, $V_{mp,ref}$, $I_{mp,ref}$, R_{so} and R_{sho} are range-scaled in order to delimit the *I–V* characteristic between the unity values of voltage and current. Range-scaling is achieved by dividing the voltage data by $V_{oc,ref}$, the current data by $I_{sc,ref}$ and the resistance data by the ratio of $V_{oc,ref}$ and $I_{sc,ref}$. The thermal correction factor K is used to slide the *I–V* characteristic at irradiance G_{ref} on the *V* axis in order to better fit the characteristics issued by the manufacturer at temperatures $T^* \neq T_{ref}$. Factor K is calculated with the formal imposition that the *I–V* characteristic evaluated with Equation (26) at G_{ref} and at the selected temperature T^* must contain the MPP issued by the manufacturer for the same T^*. The value of T^* to be used to determine K should be chosen considering the maximum or the minimum expected working temperature of the PV module and, obviously, the data provided by the manufacturer. Photocurrent $I_L(T)$ and reverse saturation current $I_0(\alpha_G, T)$ are calculated with the following expressions:

$$I_L(T) = I_{L,ref} + \mu_{I,sc}\left(T - T_{ref}\right) \tag{A71}$$

$$I_0(\alpha_G, T) = \exp\left[\frac{\alpha_G - 0.2}{1 - 0.2}\ln\frac{I_0(1, T)}{I_0(0.2, T)} + \ln I_0(0.2, T)\right] \tag{A72}$$

that is obtained with the logarithmical interpolation of the value of $I_0(1, T)$, calculated with for $G = G_{ref}$ ($\alpha_G = 1$), and the value of $I_0(0.2, T)$, calculated for $G = 200 \text{ W/m}^2$ ($\alpha_G = 0.2$). Both $I_0(1, T)$ and $I_0(0.2, T)$ can be evaluated with the following equation, which refers to the open circuit point:

$$I_0(\alpha_G, T) = \alpha_G\left[\frac{I_L(T) - V_{oc}(\alpha_G, T)/R_{sh,ref}}{e^{\frac{V_{oc}(\alpha_G, T)}{nT}} - 1}\right] \tag{A73}$$

Open circuit voltage $V_{oc}(\alpha_G, T)$ is calculated by means of the expression:

$$V_{oc}(\alpha_G, T) = V_{oc}(\alpha_G, T_{ref}) + \mu_{V,oc}\left(T - T_{ref}\right) \tag{A74}$$

To calculate $I_0(1, T)$ and $I_0(0.2, T)$ with Equation (A73), the values of $V_{oc}(1, T_{ref})$ and $V_{oc}(0.2, T_{ref})$ must be used in Equation (A74). The values of $V_{oc}(1, T_{ref})$ correspond to $V_{oc,ref}$, whereas the value of $V_{oc}(0.2, T_{ref})$ has to be extracted from the *I-V* curves issued by the manufacturer at $G = 200$ W/m^2 and $T = T_{ref}$.

A9. Seddaoui, Rahmani, Kessal and Chauder Model

The hypotheses and equations of the model of Phang *et al.* are used and the model parameters are calculated by means of the procedure proposed by Hadj Arab *et al.* Unlike the Hadj Arab *et al.* model, to calculate the *I-V* characteristics for conditions different from the SRC, reverse saturation current $I_0(T)$ was calculated with the following expressions:

$$I_0(T) = I_{0,ref}\left(\frac{T}{T_{ref}}\right)^3 e^{\frac{\varepsilon_G N_{cs}}{n}\left(\frac{1}{T_{ref}} - \frac{1}{T}\right)} \tag{A75}$$

whereas, for shunt resistance R_{sh} and photocurrent $I_L(G, T)$, Equation (A38) and (A62) were used.

A10. Siddique, Xu and De Doncker Model

The following equations can be obtained by solving Equations (A4) and (A5), which refer to the short circuit and open circuit conditions:

$$I_{0,ref} = \frac{\left(1 + \frac{R_s}{R_{sh}}\right) I_{0,ref} - \frac{V_{oc,ref}}{R_{sh}}}{e^{\frac{V_{oc,ref}}{nT_{ref}}} - e^{\frac{I_{sc,ref}R_s}{nT_{ref}}}} \tag{A76}$$

$$I_{L,ref} = \frac{\left(1 + \frac{R_s}{R_{sh}}\right) I_{0,ref}\left(e^{\frac{V_{oc,ref}}{nT_{ref}}} - 1\right) + \frac{V_{oc,ref}}{R_{sh}}\left(1 - e^{\frac{I_{sc,ref}R_s}{nT_{ref}}}\right)}{e^{\frac{V_{oc,ref}}{nT_{ref}}} - e^{\frac{I_{sc,ref}R_s}{nT_{ref}}}} \tag{A77}$$

If the previous equations are substituted in Equation (A9), which describes the third piece of information, resistance R_{sh} can be calculated with the following expression:

$$R_{sh} = \frac{R_s\left(I_{sc,ref} - I_{mp,ref}\right) - V_{mp,ref} - \left(R_s I_{sc,ref} - V_{oc,ref}\right)B/A}{I_{mp,ref} - I_{sc,ref}\left(1 - B/A\right)} \tag{A78}$$

in which it is:

$$A = e^{\frac{V_{oc,ref}}{nT_{ref}}} - e^{\frac{I_{sc,ref}R_s}{nT_{ref}}} \tag{A79}$$

$$B = e^{\frac{V_{mp,ref} + I_{mp,ref}R}{nT_{ref}}} - e^{\frac{I_{sc,ref}R_s}{nT_{ref}}} \tag{A80}$$

The following equation can be analogously extracted from Equation (A1) and (A25):

$$R_{sh} = \frac{V_{mp,ref} - I_{mp,ref}R_s + C\frac{I_{sc,ref}R_s - V_{oc,ref}}{A} - \left(V_{mp,ref} - I_{mp,ref}R_s\right)}{I_{mp,ref} + \frac{I_{sc,ref}C}{A}\left(I_{mp,ref}R_s - V_{mp,ref}\right)} \tag{A81}$$

where it is:

$$C = \frac{e^{\frac{V_{mp,ref}+I_{mp,ref}R_s}{nT_{ref}}}}{nT_{ref}} \tag{A82}$$

From Equations (A78) and (A81), the following relation is obtained:

$$\frac{R_s\left(I_{sc,ref}-I_{mp,ref}\right)-V_{mp,ref}-\left(R_sI_{sc,ref}-V_{oc,ref}\right)B/A}{I_{mp,ref}-I_{sc,ref}\left(1-B/A\right)}+ \\ -\frac{V_{mp,ref}-I_{mp,ref}R_s+C\frac{I_{sc,ref}R_s-V_{oc,ref}}{A}-\left(V_{mp,ref}-I_{mp,ref}R_s\right)}{I_{mp,ref}+\frac{I_{sc,ref}C}{A}\left(I_{mp,ref}R_s-V_{mp,ref}\right)} = 0 \tag{A83}$$

Only the values of R_s contained into the following range:

$$R_{s,min} = 0 \qquad R_{s,max} = \frac{V_{oc,ref}-V_{mp,ref}}{I_{mp,ref}} \tag{A84}$$

are valid, whereas the shunt resistance, which can be calculated using either Equation (A78) or Equation (A81), should not exceed the minimum value given by:

$$R_{sh,min} = \frac{V_{mp,ref}}{I_{sc,ref}-I_{mp,ref}} \tag{A85}$$

The model parameters are calculated with the following steps:

(1) the initial value $a = 1$ is set and $n = N_{cs}k/q$ is used;
(2) R_s is calculated by Equation (A83);
(3) if it is $R_s < R_{s,min}$ or $R_s > R_{s,max}$, the value of parameter a is slightly increased and step 2 is repeated;
(4) if it is $R_{s,min} \leqslant R_s \leqslant R_{s,max}$, then:
(5) R_{sh} is calculated by Equation (A78);
(6) $I_{0,ref}$ is calculated by Equation (A76);
(7) $I_{L,ref}$ is calculated by Equation (A77);
(8) if it is $R_{sh} < R_{sh,min}$ or $I_{0,ref} \leqslant 0$ or $I_{L,ref} \leqslant I_{sc,ref}$, the value of a is slightly increased and steps 2, 3, 4, 5, 6 and 7 are repeated;
(9) if it is $R_{sh} \geqslant R_{sh,min}$ and $I_{0,ref} > 0$ and $I_{L,ref} > I_{sc,ref}$ then:
(10) Equation (2) is calculated in order to find the maximum power point;
(11) the calculated maximum power is compared with the issued value of $P_{mp,ref}$;
(12) the whole iterative procedure is repeated by slightly incrementing n until it is found the condition in which the minimum difference between the calculated maximum power and the issued value of $P_{mp,ref}$ is reached.

The dependence on values of solar irradiance and cell temperature different from the SRC is considered using Equations (A62) and (A30), for the photocurrent and the reverse saturation current, respectively. The open circuit voltage is described with the following expression:

$$V_{oc}(G,T) = V_{oc,ref} + \mu_{V,oc}\left(T-T_{ref}\right) + nT\ln\left(\frac{G}{G_{ref}}\right) \tag{A86}$$

which was proposed by Chenlo *et al.* [86].

A11. Yetayew and Jyothsna Model

Points *A* and *B* are selected on the *I-V* characteristic at the SRC in correspondence of the following voltage values:

$$V_A = \frac{V_{oc,ref}}{2} \qquad V_B = \frac{V_{mp,ref} + V_{oc,ref}}{2} \tag{A87}$$

The above five pieces of information permit to write five independent versions of Equation (2) that are solved by means of the Newton-Raphson method. In order to consider the effects of conditions different from the SRC, Equations (A30), (A62) and (A38) are used to describe parameters $I_0(T)$, $I_L(G,T)$ and $R_{sh}(G)$.

A12. Orioli and Di Gangi model

If the following hypotheses are assumed:

$$e^{\frac{I_{sc,ref} R_{s,ref}}{n T_{ref}}} \approx 1 \qquad R_{s,ref} << R_{sh,ref} \qquad \frac{I_{0,ref}}{n T_{ref}} e^{\frac{I_{sc,ref} R_{s,ref}}{n T_{ref}}} << \frac{1}{R_{sh,ref}} \tag{A88}$$

the photocurrent and the shunt resistance can be calculated with the following expressions obtained from Equations (A4) and (A6), which describe the conditions related to the short circuit point and the derivative of current at the short circuit point:

$$I_{L,ref} = I_{sc,ref} \tag{A89}$$

$$R_{sh,ref} = R_{sho} \tag{A90}$$

Using the previous equations in Equation (A5), which describes the open circuit condition, the following expression can be obtained:

$$I_{0,ref} = \frac{I_{sc,ref} - \frac{V_{oc,ref}}{R_{sho}}}{e^{\frac{V_{oc,ref}}{n T_{ref}}} - 1} \tag{A91}$$

If Equations (A89), (A90) and (A91) are used in Equation (A9), which contains the MPP condition, and the following hypotheses are adopted:

$$e^{\frac{V_{mp,ref} + I_{mp,ref} R_{s,ref}}{n T_{ref}}} >> 1 \qquad e^{\frac{V_{oc,ref}}{n T_{ref}}} >> 1 \tag{A92}$$

it is possible to extract the following expression for parameter *n*:

$$n = \frac{V_{mp,ref} + I_{mp,ref} R_{s,ref} - V_{oc,ref}}{T_{ref} \ln \left[\frac{(I_{sc,ref} - I_{mp,ref}) R_{sho} - (V_{mp,ref} + I_{mp,ref} R_{s,ref})}{I_{sc,ref} R_{sho} - V_{oc,ref}} \right]} \tag{A93}$$

The fifth piece of the used information is expressed by the equation:

$$\left. \frac{\partial I}{\partial V} \right|_{\substack{V = V_{oc,ref} \\ I = 0}} = -\frac{\frac{I_{0,ref}}{n T_{ref}} e^{\frac{V_{oc,ref}}{n T_{ref}}} + \frac{1}{R_{sho}}}{1 + R_{s,ref} \left(\frac{I_{0,ref}}{n T_{ref}} e^{\frac{V_{oc,ref}}{n T_{ref}}} + \frac{1}{R_{sho}} \right)} = -\frac{1}{R_{so}} \tag{A94}$$

To calculate the model parameters, the following sequence of steps is adopted:

(1)　$I_{L,ref}$ is calculated by Equation (A89);

(2) $R_{sh,ref}$ is calculated by Equation (A90);

(3) $I_{0,ref}$ is calculated by Equation (A91);

(4) an initial values of $R_{s,ref}$ is assumed;

(5) n is calculated by Equation (A93);

(6) Equation (A94) is calculated;

(7) the iterative procedure is concluded if Equation (A94) is verified within a fixed accuracy; otherwise, a new value of $R_{s,ref}$ is assumed and steps 5, 6, and 7 are repeated.

Unlike the Lo Brano *et al.* model, factor *K* is calculated with the formal imposition that the *I–V* characteristic evaluated by Equation (26), at G_{ref} and at a selected temperature $T^* \neq T_{ref}$, must reach the MPP in correspondence of the same voltage for which the MPP is reached on the *I-V* curve issued by the manufacturer for $G = G_{ref}$ and $T = T^*$.The value of T^* to be used to determine *K* is chosen considering the maximum or the minimum expected working temperature of the PV module and, obviously, the data provided by the manufacturer. In order to avoid the graphical extraction of R_{so} and R_{sho}, the following empirical relations are proposed:

$$R_{so} = C_s \frac{V_{oc,ref}}{I_{sc,ref}} \tag{A95}$$

$$R_{sho} = C_{sh} \frac{V_{oc,ref}}{I_{sc,ref}} \tag{A96}$$

in which $C_s = 0.11175$; $C_{sh} = 34.49692$, for mono and polycrystalline PV panels, $C_s = 0.16129$; $C_{sh} = 124.48114$, for HIT PV modules. The diode reverse saturation current is calculated with the following equation:

$$I_0(\alpha_G, T) = \alpha_G \left[\frac{I_L(T) - V_{oc}(\alpha_G, T)/R_{sho}}{e^{\frac{V_{oc}(\alpha_G,T)}{nT}} - 1} \right] \tag{A97}$$

which refers to the open circuit point. Open circuit voltage $V_{oc}(\alpha_G,T)$ is evuluated by means of the following empirical expression:

$$V_{oc}(\alpha_G, T) = V_{oc,ref} \left\{ 1 + C_1 \ln(\alpha_G) + C_2 \left[\ln(\alpha_G)\right]^2 + C_3 \left[\ln(\alpha_G)\right]^3 \right\} + \mu_{V,oc}(T - T_{ref}) \tag{A98}$$

where: $C_1 = 5.468511 \times 10^{-2}$, $C_2 = 5.973869 \times 10^{-3}$ and $C_3 = 7.616178 \times 10^{-4}$.

References

1. Yu, G.J.; Jung, Y.S.; Choi, J.Y.; Kim, G.S. A novel two-mode MPPT control algorithm based on comparative study of existing algorithms. *Sol. Energy* **2004**, *76*, 455–463. [CrossRef]

2. Femia, N.; Petrone, G.; Spagnuolo, G.; Vitelli, M. Optimization of perturb and observe maximum power point tracking method. *IEEE Trans. Power Electron.* **2005**, *20*, 963–973. [CrossRef]

3. Liu, Y.H.; Huang, J.W. A fast and low cost analog maximum power point tracking method for low power photovoltaic systems. *Sol. Energy* **2011**, *85*, 2771–2780. [CrossRef]

4. Bennett, T.; Zilouchian, A.; Messenger, R. Photovoltaic model and converter topology considerations for MPPT purposes. *Sol. Energy* **2012**, *86*, 2029–2040. [CrossRef]

5. Ciulla, G.; Lo Brano, V.; Di Dio, V.; Cipriani, G. A comparison of different one-diode models for the reresentation of I-V characteristic of a PV cell. *Renew. Sustain. Energy Rev.* **2014**, *32*, 684–696. [CrossRef]

6. Goetzberger, A.; Knobloch, J.; Voss, B. *Crystalline Silicon Solar Cells*; John Wiley & Sons: Chichester, UK, 1998.

7. Shockley, W. *Electrons and Holes in Semiconductors*; Van Nostrand: New York, NY, USA, 1950.

8. Millman, J.; Halkias, C.C. *Electronic Devices and Circuits*; McGrow-Hill: New York, NY, USA, 1967.

9. Wolf, M.; Rauscenbach, H. Series Resistance Effects on Solar Cell Measurements. *Adv. Energy Convers.* **1963**, *3*, 455–479. [CrossRef]

10. Chan, D.S.H.; Phang, J.C.H. Analytical methods for the extraction of solar-cell single- and double-diode model parameters from *I-V* characteristics. *IEEE Trans. Electron Devices* **1987**, *34*, 286–293. [CrossRef]

11. Enebish, N.; Agchbayar, D.; Dorjkhand, S.; Baatar, D.; Ylemj, I. Numerical analysis of solar cell current-voltage characteristics. *Sol. Energy Mater. Sol. Cells* **1993**, *29*, 201–208. [CrossRef]

12. Hovinen, A. Fitting of the solar cell IV-curve to the two diode model. *Phys. Scr.* **1994**, *T54*, 175–176. [CrossRef]

13. Garrido-Alzar, C.L. Algorithm for extraction of solar cell parameters from *I-V* curve using double exponential model. *Renew. Energy* **1997**, *10*, 125–128. [CrossRef]

14. Zhao, R.; Xu, H.-J.; Zhao, Z.-Y.; Zhang, S.-H. A simplified double-exponential model of potovoltaic module in Matlab™. In Proceedings of the International Conference on Energy and Environment Technology, ICEET '09, Guilin, China, 16–18 October 2009; pp. 157–160.

15. Yordanov, G.H.; Midtgård, O.M.; Saetre, T.O. Two-diode model revisited: parameters extraction from semi-log plots of I-V data. In Proceedings of the 25th European Photovoltaic Solar Energy Conference and Exhibition/5th World Conference on Photovoltaic Energy Conversion, Valencia, Spain, 6–10 September 2010; pp. 4156–4163.

16. Yordanov, G.H.; Midtgård, O.M.; Saetre, T.O. Extracting parameters from semi-log plots of polycrystalline silicon PV modules outdoor I-V data: Double-exponential model revisited. In Proceedings of the 35th IEEE Photovoltaic Specialists Conference (PVSC), Honolulu, HI, USA, 20–25 June 2010; pp. 2756–2761.

17. Ishaque, K.; Salam, Z.; Taheri, H. Simple, fast and accurate two-diode model for photovoltaic modules. *Sol. Energy Mater. Sol. Cells* **2011**, *95*, 586–594. [CrossRef]

18. Gupta, S.; Tiwari, H.; Fozdar, M.; Chandna, V. Development of a two diode model for photovoltaic modules suitable for use in simulation studies. In Proceedings of the Asia–Pacific Power and Energy Engineering Conference (APPEEC), Shanghai, China, 27–29 March 2012; pp. 1–4.

19. Maoucha, A.; Djeffal, F.; Arar, D.; Lakhdar, N.; Bendib, T.; Abdi, M.A. An accurate organic solar cell parameters extraction approach based on the illuminated I–V characteristics for double diode modelling. In Proceedings of the First International Conference on renewable Energies and Vehicular Technology (REVET), Hammamet, Tunisia, 26–28 March 2012; pp. 74–77.

20. Hejri, M.; Mokhtari, H.; Azizian, M.R.; Ghandhari, M.; Söder, L. On the parameter extraction of a five-parameter double-diode model of photovoltaic cells and modules. *IEEE J. Photovolt.* **2014**, *4*, 915–923. [CrossRef]

21. Babu, B.C.; Gurjar, S. A novel simplified two-diode model of photovoltaic (PV) module. *IEEE J. Photovolt.* **2014**, *4*, 1156–1161. [CrossRef]

22. Ikegami, T.; Maezono, T.; Nakanishi, F.; Yamagata, Y.; Ebihara, K. Estimation of equivalent circuit parameters of PV module and its application to optimal operation of PV system. *Sol. Energy Mater. Sol. Cells* **2001**, *67*, 389–395. [CrossRef]

23. De Blas, M.A.; Torres, J.L.; Prieto, E.; Garcia, A. Selecting a suitable model for characterizing photovoltaic devices. *Renew. Energy* **2002**, *25*, 371–380.

24. Hadj Arab, A.; Chenlo, F.; Benghanem, M. Loss-of-load probability of photovoltaic water pumping systems. *Sol. Energy* **2004**, *76*, 713–723. [CrossRef]

25. De Soto, W.; Klein, S.A.; Beckman, W.A. Improvement and validation of a model for photovoltaic array performance. *Sol. Energy* **2006**, *80*, 78–88. [CrossRef]

26. Sera, D.; Teodorescu, R.; Rodriguez, P. PV panel model based on datasheet values. In Proceedings of the IEEE International Symposium on Industrial Electronics, ISIE, Vigo, Spain, 4–7 June 2007; pp. 2392–2396.

27. Villalva, M.G.; Gazoli, J.R.; Filho, E.R. Comprehensive approach to modeling and simulation of photovoltaic arrays. *IEEE Trans. Power Electron.* **2009**, *24*, 1198–1208. [CrossRef]

28. Coelho, R.F.; Cancer, F.; Martins, D.C. A proposed photovoltaic module and array mathematical modeling destined to simulation. In Proceedings of the IEEE International Symposium on Industrial Electronics (ISIE), Seoul, Korea, 5–8 July 2009; pp. 1624–1629.

29. Lo Brano, V.; Orioli, A.; Ciulla, G.; Di Gangi, A. An improved five-parameter model for photovoltaic modules. *Sol. Energy Mater. Sol. Cells* **2010**, *94*, 1358–1370. [CrossRef]

30. Kim, W.; Choi, W. A novel parameter extraction method for the one-diode solar cell model. *Sol. Energy* **2010**, *84*, 1008–1019. [CrossRef]

31. Farivar, G.; Asaei, B. Photovoltaic module single diode model parameters extraction based on manufacturer datasheet parameters. In Proceedings of the IEEE International Conference on Power and Energy (PECon), Kuala Lumpur, Malaysia, 29 November–1 December 2010; pp. 929–934.

32. Carrero, C.; Ramírez, D.; Rodríguez, J.; Platero, C.A. Accurate and fast convergence method for parameter estimation of PV generators based on three main points of the *I-V* curve. *Renew. Energy* **2011**, *36*, 2972–2977. [CrossRef]

33. Chatterjee, A.; Keyhani, A.; Kapoor, D. Identification of photovoltaic source models. *IEEE Trans. Energy Convers.* **2011**, *26*, 883–889. [CrossRef]

34. Farret, F.A.; Lenz, J.M.; Trapp, J.G. New methodology to determinate photovoltaic parameters of solar panels. In Proceedings of the Brazilian Power Electronics Conference (COBEP), Praiamar, Brazil, 11–15 September 2011; pp. 275–279.

35. Seddaoui, N.; Rahmani, L.; Kessal, A.; Chauder, A. Parameters extraction of photovoltaic module at reference and real conditions. In Proceedings of the 46th International Universities' Power Engineering Conference (UPEC), Soest, Germany, 5–8 September 2011; pp. 1–6.

36. Katsanevakis, M. Modelling the photovoltaic module. In Proceedings of the IEEE International Symposium on Industrial Electronics (ISIE), Gdansk, Poland, 27–30 June 2011; pp. 1414–1419.

37. Lo Brano, V.; Orioli, A.; Ciulla, G. On the experimental validation of an improved five-parameter model for silicon photovoltaic modules. *Sol. Energy Mater. Sol. Cells* **2012**, *105*, 27–39. [CrossRef]

38. Lineykin, S.; Averbukh, M.; Kuperman, A. A five-parameter model of photovoltaic cell based on STC data and dimensionless. In Proceedings of the IEEE 27th Convention of Electrical & Electronics Engineers in Israel (IEEEI), Eilat, Israel, 14–17 November 2012; pp. 1–5.

39. Can, H.; Ickilli, D.; Parlak, K.S. A new numerical solution approach for the real-time modeling of photovoltaic panels. In Proceedings of the Asia-Pacific Power and Energy Engineering Conference (APPEEC), Shanghai, China, 27–29 March 2012; pp. 1–4.

40. Ahmad, M.; Talukder, A.; Tanni, M.A. Estimation of important parameters of photovoltaic modules from manufacturer's datasheet. In Proceedings of the International Conference on Informatics, Electronics & Vision (ICIEV), Dhaka, Bangladesh, 18–19 May 2012; pp. 571–576.

41. Mahmoud, S.A.; Mohamed, H.N. Novel modeling approach for photovoltaic arrays. In Proceedings of the IEEE 55th International Midwest Symposium on Circuits and Systems (MWSCAS), Boise, ID, USA, 5–8 August 2012; pp. 790–793.

42. Sangsawang, V.; Chaitusanel, S. Modeling of photovoltaic module from commercial specification in datasheet. In Proceedings of the 9th International Conference on Electrical Engineering/Electronics, Computer, Telecommunications and Information Technology (ECTI-CON), Phetchaburi, Thailand, 16–18 May 2012; pp. 1–4.

43. Tian, H.; Mancilla-David, F.; Ellis, K.; Muljadi, E.; Jenkins, P. A cell-to-module-to-array detailed model for photovoltaic panels. *Sol. Energy* **2012**, *86*, 2695–2706. [CrossRef]

44. Orioli, A.; Di Gangi, A. A procedure to calculate the five-parameter model of crystalline silicon photovoltaic modules on the basis of the tabular performance data. *Appl. Energy* **2013**, *102*, 1160–1177. [CrossRef]

45. Islam, M.A.; Merabet, A.; Beguenane, R.; Ibrahim, H. Modeling solar photovoltaic cell and simulated performance analysis of a 250W PV module. In Proceedings of the IEEE Electrical Power & Energy Conference (EPEC), Halifax, NS, Canada, 21–23 August 2013; pp. 1–6.

46. Jena, D.; Ramana, V.V. Simple and accurate method of modelling photovoltaic module: A different approach. In Proceedings of the International Conference on Green Computing, Communication and Conservation of Energy (ICGCE), Chennai, India, 12–14 December 2013; pp. 465–469.

47. Mahmoud, Y.; Xiao, W.; Zeineldin, H.H. A simple approach to modeling and simulation of photovoltaic modules. *IEEE Trans. Sustain. Energy* **2012**, *3*, 185–186. [CrossRef]

48. Mahmoud, Y.; Xiao, W.; Zeineldin, H.H. A parameterization approach for enhancing PV model accuracy. *IEEE Trans. Ind. Electron.* **2013**, *60*, 5708–5716. [CrossRef]

49. Siddique, H.A.B.; Xu, P.; De Doncker, R.W. Parameter extraction algorithm for one-diode model of PV panels based on datasheet values. In Proceedings of the International Conference on Clean Electrical Power (ICCEP), Alghero, Italy, 11–13 June 2013; pp. 7–13.

50. Siddiqui, M.U.; Arif, A.F.M.; Bilton, A.M.; Dubowsky, S.; Elshafei, M. An improved electric circuit model for photovoltaic modules based on sensitivity analysis. *Sol. Energy* **2013**, *90*, 29–42. [CrossRef]

51.　Tian, H.; Mancilla-David, F.; Muljadi, E.; Stoffel, T.; Andreas, A. Model validation of photovoltaic systems. In Proceedings of the IEEE Green Technologies Conference, Denver, CO, USA, 4–5 April 2013; pp. 93–97.

52.　Yetayew, T.T.; Jyothsna, T.R. Improved single-diode modeling approach for photovoltaic modules using data sheet. In Annual IEEE India Conference (INDICON), Mumbai, India, 13–15 December 2013; pp. 1–6.

53.　Bai, J.; Liu, S.; Hao, Y.; Zhang, Z.; Jiang, M.; Zhang, Y. Development of a new compound method to extract the five parameters of PV modules. *Energy Convers. Manag.* **2014**, *79*, 294–303. [CrossRef]

54.　Cubas, J.; Pindado, S.; Victoria, M. On the analytical approach for modeling photovoltaic systems behaviour. *J. Power Sources* **2014**, *247*, 467–474. [CrossRef]

55.　Lineykin, S.; Averbukh, M.; Kuperman, A. An improved approach to extract the single-diode equivalent circuit parameters of a photovoltaic cell/panel. *Renew. Sustain. Energy Rev.* **2014**, *30*, 282–289. [CrossRef]

56.　Ma, T.; Yang, H.; Lu, L. Development of a model to simulate the performance characteristics of crystalline silicon photovoltaic modules/strings/arrays. *Sol. Energy* **2014**, *100*, 31–41. [CrossRef]

57.　Xu, Y.; Kong, X.; Zeng, Y.; Tao, S.; Xiao, X. A modeling method for photovoltaic cells using explicit equations and optimization algorithm. *Electr. Power Energy Syst.* **2014**, *59*, 23–28. [CrossRef]

58.　Jervase, J.A.; Bourdoucen, H.; Al-Lawati, A. Solar cell parameter extraction using genetic algorithms. *Meas. Sci. Technol.* **2001**, *12*, 1922–1925. [CrossRef]

59.　Jain, A.; Kapoor, A. Exact analytical solutions of the parameters of real solar cells using Lambert W-function. *Sol. Energy Mater. Sol. Cells* **2004**, *81*, 269–277. [CrossRef]

60.　Ortiz-Conde, A.; García Sanchez, F.J.; Muci, J. New method to extract the model parameters of solar cells from the explicit analytic solutions of their illuminated I–V characteristics. *Sol. Energy Mater. Sol. Cells* **2006**, *90*, 352–361. [CrossRef]

61.　Mekki, H.; Mellit, A.; Salhi, H.; Khaled, B. Modeling and simulation of photovoltaic panel based on artificial neural networks and VHDL-language. In Proceedings of the 14th IEEE International Conference on Electronics, Circuits and Systems, ICECS, Marrakech, Morocco, 11–14 December 2007; pp. 58–61.

62.　Moldovan, N.; Picos, R.; Garcia-Moreno, E. Parameter extraction of a solar cell compact model using genetic algorithms. In Spanish Conference on Electron Devices, CDE, Santiago de Compostela, Spain, 11–13 Feburay 2009; pp. 379–392.

63.　Zagrouba, M.; Sellami, A.; Bouaïcha, M.; Ksouri, M. Identification of PV solar cells and modules parameters using the genetic algorithms: Application to maximum power extraction. *Sol. Energy* **2010**, *84*, 860–866. [CrossRef]

64.　Sandrolini, L.; Artioli, M.; Reggiani, U. Numerical method for the extraction of photovoltaic module double-diode model parameters through cluster analysis. *Appl. Energy* **2010**, *87*, 442–451. [CrossRef]

65.　Ishaque, K.; Salam, Z.; Taheri, H.; Shamsudin, A. A critical evaluation of EA computational methods for photovoltaic cell parameter extraction based on two-diode. *Sol. Energy* **2011**, *85*, 1768–1779. [CrossRef]

66.　Ishaque, K.; Salam, Z. An improved modelling method to determine the model parameters of photovoltaic (PV) modules using differential evolution (DE). *Sol. Energy* **2011**, *85*, 2349–2359. [CrossRef]

67.　Askarzadeh, A.; Rezazadeh, A. Parameter identification for solar cell models using harmony search-based algorithms. *Sol. Energy* **2012**, *84*, 3241–3249. [CrossRef]

68.　Toledo, F.J.; Blanes, J.M.; Garrigós, A.; Martínez, J.A. Analytical resolution of the electrical four-parameters model of a photovoltaic module using small perturbation around the operating point. *Renew. Energy* **2012**, *43*, 83–89. [CrossRef]

69.　Lun, S.; Du, C.; Yang, G.; Wang, S.; Guo, T.; Sang, J.; Li, J. An explicit approximate I–V characteristic model of a solar cell based on padé approximants. *Sol. Energy* **2013**, *92*, 147–159. [CrossRef]

70.　Merten, J.; Asensi, J.M.; Voz, C.; Shah, A.V.; Platz, R.; Andreu, J. Improved equivalent circuit and analytical model for amorphous silicon solar cells and modules. *IEEE Trans. Electron Devices* **1998**, *45*, 423–429. [CrossRef]

71.　Burgelman, M.; Niemegeers, A. Calculation of CIS and CdTe module efficiencies. *Sol. Energy Mater. Sol. Cells* **1998**, *51*, 129–143. [CrossRef]

72.　Stutenbaeumer, U.; Mesfin, B. Equivalent model of monocrystalline, polycrystalline and amorphous silicon solar cells. *Renew. Energy* **1999**, *18*, 501–512. [CrossRef]

73.　Brecl, K.; Krc, J.; Smole, F.; Topic, M. Simulating tandem solar cells. In Proceedings of the 3rd World Conference on Photovoltaic Energy Conversion, Osaka, Japan, 11–18 May 2003; Volume 1, pp. 499–502.

74. Xiao, W.; Dunford, W.G.; Capel, A. A novel modeling method for photovoltaic cells. In Proceedings of the IEEE 35th Annual Power Electronics Specialists Conference (PESC 04), Aachen, Germany, 20–25 June 2004; pp. 1950–1956.

75. Burgelman, M.; Verschraegen, J.; Degrave, S.; Nollet, P. Modeling thin-film PV devices. *Prog. Photovolt.* **2004**, *12*, 143–153. [CrossRef]

76. Werner, B.A.; Prorok, M. Analysis of the applicability of the diode equivalent model for GIGS thin-film photovoltaic modules. In Proceedings of the Photonics and Microsystems, International Students and Young Scientists Workshop, Wroclaw, Porland, 30 June–2 July 2006; pp. 66–68.

77. Werner, B.; Zdanowicz, T. Experimental determination of physical parameters in CIGS solar cells. In Proceedings of the International Students and Young Scientists Workshop on Photonics and Microsystems, Dresden, Germany, 8–10 July 2007; pp. 84–86.

78. Ahmad, S.; Mittal, N.R.; Bhattacharya, A.B.; Singh, M. Simulation, output power optimization and comparative study of silicon and thin film solar cell modules. In Proceedings of the 5th IEEE Conference on Industrial Electronics and Applications (ICIEA), Taichung, Taiwan, 15–17 June 2010; pp. 624–629.

79. Janssen, G.J.M.; Slooff, L.H.; Bende, E.E. 2D—Finite element model of a CIGS module. In Proceedings of the 2012 38th IEEE Photovoltaic Specialists Conference (PVSC), Austin, TX, USA, 3–8 June 2012; pp. 1481–1485.

80. Molina-Garcia, A.; Bueso, M.C.; Kessler, M.; Guerrero-Perez, J.; Fuentes, J.A.; Gomez-Lazaro, E. CdTe thin-film solar module modeling using a non–linear regression approach. In Proceedings of the 17th Power Systems Computation Conference, Stockholm, Sweden, 22–26 August 2011.

81. Ferdández, E.F.; Siefer, G.; Almonacid, F.; García Loureiro, A.J.; Pérez-Higueras, P. A two subcell equivalent solar cell model for III-V triple junction solar cells under spectrum and temperature variations. *Sol. Energy* **2013**, *92*, 221–229. [CrossRef]

82. Parisi, A.; Curcio, L.; Rocca, V.; Stivala, S.; Cino, A.C.; Busacca, A.C.; Cipriani, G.; La Cascia, D.; Di Dio, V.; Miceli, R. Photovoltaic module characteristics from CIGS solar cell modelling. In Proceedings of the International Conference on Renewable Energy Research and Applications (ICRERA), Madrid, Spain, 20–23 October 2013; pp. 1139–1144.

83. Markvart, T.; Costañer, L. Solar cells. In *Materials, Manufacture and Operation*; Elsevier: Oxford, UK, 2005.

84. Kennerud, K.L. Analysis of performance degradation in CdS solar cells. *IEEE Trans. Aerosp. Electronic Syst.* **1969**, *5*, 912–917. [CrossRef]

85. Phang, J.C.H.; Chan, D.S.H.; Phillips, J.R. Accurate analytical method for the extraction of solar cell model parameters. *Electron. Lett.* **1984**, *20*, 406–408. [CrossRef]

86. Klein, S. EES—Engineering Equation Solver, F-Chart Software. 2005. Available online: http://www.fchart.com (accessed on 26 May 2016).

87. Laudani, A.; Riganti Fulginei, F.; Salvini, A. Identification of the one-diode model for photovoltaic modules from datasheet values. *Sol. Energy* **2014**, *108*, 432–446. [CrossRef]

88. Townsend, T.U. A Method for Estimating the Long-Term Performance of Direct-Coupled Photovoltaic Systems. Master's Thesis, Mechanical Engineering, University of Wisconsin-Madison, Madison, WI, USA, 1989.

89. Chenlo, F.; Fabero, F.; Alonso, M.C. *A Comparative Study between Indoor and Outdoor Measurements*; Final Report of Project: Testing, Norms, Reliability and Harmonisation, Joule II—Contract No. JOU2-CT92–0178; European Commission: Brussels, Belgium, 1995.